https://doi.org/10.5194/egusphere-2026-524
Preprint. Discussion started: 10 February 2026

Building a random forest machine learning model for carbon budget estimation in agricultural fields using discontinuous atmospheric Eddy Covariance measurements.

Camille Pery[1,2*], Pierre Polsenaere[1], Eric Lamaud[2], Natacha Volto[3], Nathalie Long[3], Jonathan Deborde[1], Shunko Bolsée[2], Olivier Philippine[6], Vona Méléder[4,5], Christine Dupuy[3]

[1] Ifremer, COAST, 17390 La Tremblade, France
[2] INRAe, ISPA, 33140 Villenave D'Ornon, France
[3] LIENSs, UMR7266 CNRS- La Rochelle Université, 17000 La Rochelle, France
[4] Nantes Université, ISOMer, 44000 Nantes, France
[5] Institut Universitaire de France, IUF, France
[6] Unima, 17180 Périgny, France

Correspondence to: Camille Pery (camille.pery@bordeaux-inp.fr)

**Present address:* Univ. Bordeaux, CNRS, Bordeaux INP, UMR 5805, F-33600 Pessac, France

Abstract. Atmospheric CO_2 exchanges in agroecosystems are strongly controlled by plant phenology, management and microclimatic conditions, yet obtaining finely resolved flux estimates across heterogeneous agricultural landscapes remains challenging. This study evaluates the ability of a single Eddy Covariance (EC) system combined with wind-sector partitioning and Random Forest (RF) modelling to estimate annual carbon budgets of adjacent fields (wheat, mixed-grain, permanent grassland) in the Marais Poitevin wetland. Fluxes were measured over the period 2023-01-01-2024-01-31 and attributed to the different fields by wind sectors. Two modelling strategies were compared (i) a single global RF trained on all sectors and (ii) sector-specific RFs for each adjacent field. RF models globally showed good overall performance ($R^2 \approx 0.68$-0.95 depending on sector), while the sectoral approach better reproduced phenological dynamics and responses to management events (harvest, grazing) than the global model, which tended to smooth site-specific signals. Annual carbon budgets estimated from the sectoral models indicate that the permanent grassland and the wheat field acted as net sinks (-259 and -216 g C m^{-2} yr^{-1}, respectively), whereas the mixed grain and the hybrid field behaved as net sources (+182 and +231 g C m^{-2} yr^{-1}). Main limitations include spatial attribution uncertainty related to the EC footprint under stable conditions, flux disturbances during stormy episodes, and the limited one-year observation period. This study highlights the novelty and practical value of coupling a single EC system with wind-sector partitioning and machine learning approaches to resolve carbon fluxes at the field scale within heterogeneous agricultural landscapes. This integrated approach provides a cost-effective alternative to traditional multi-tower setups, offering new opportunities to monitor spatial carbon dynamics and management effects in real agricultural mosaics. Beyond methodological innovation, the goal of this work is to establish a comprehensive carbon budget not merely for a single agroecosystem, but for the terrestrial component of a wetland area, capturing the complexity of its ecological and biogeochemical interactions.

https://doi.org/10.5194/egusphere-2026-524
Preprint. Discussion started: 10 February 2026

Keywords: Eddy Covariance, Random Forest, carbon budget, wind sectors, agriculture, gap-filling.

1 Introduction

Agricultural lands cover a vast fraction of the terrestrial biosphere with around 50% of the Earth's vegetated land surface (about 5 billion ha) under cultivation, grassland or rangeland (Zomer et al., 2017). This extensive area makes agroecosystems as a major component of the global carbon cycle. Indeed, since 1750 corresponding to the start of the industrial era, conversion of forests and meadows to cropland and grassland has released large amounts of CO_2 on the order of 214 ± 67 PgC from biomass and soils, contributing roughly to a quarter of anthropogenic greenhouse-gas emissions (Zomer et al., 2017). In the last decade, net CO_2 emissions from land-use change (mostly driven by agriculture) averaged about 4.2 ± 2.6 Gt CO_2 yr^{-1} (Friedlingstein et al., 2025). At the same time, crops and managed fields also take up significant amount of carbon from the atmosphere via photosynthesis, so agricultural ecosystems can act as both carbon sinks and sources for the atmospheric CO_2. For example, intensive agriculture can store carbon in plant biomass and soils, while conventional cropping and elimination of residues can turn fields into net sources of CO_2 due to large soil respiration rates. Globally, agricultural soils hold on the order of 8-10% of the world's soil organic carbon (Wu et al., 2024), so even small changes in land management can have measurable impacts on the atmospheric CO_2 concentration. At the same time, climate and land-use intensity control the CO_2 exchange of agroecosystems in complex and interconnected ways: solar radiation and air temperature are the primary drivers of gross primary production (GPP) in many temperate croplands (Moreaux et al., 2020), while water availability, plant phenology and vapor pressure deficit (VPD) modulate the growing-season uptake. Crop type and anthropogenic management (e.g. fertilization, irrigation, harvest) further alter the balance between photosynthesis and respiration; for instance, deep-rooted or perennial crops typically achieve higher seasonal uptake than shallow-rooted annuals, and no-harvest practices slow down soil CO_2 release. Thus, the net carbon budget of agricultural fields sensitively depends on crop species, phenological stage and local environment variables, as well as on socio-economic factors determining land-use intensity (Moreaux et al., 2020; Zomer et al., 2017).

To quantify land-atmosphere CO_2 exchange over large spatial scales and fine time resolution, the Eddy Covariance (EC) technique has become a widely used method in ecosystem science, although it remains costly and technically demanding. EC deploys fast anemometers and CO_2/H_2O Infra-Red Gaz Analysers (IRGA) on towers to directly measure the turbulent flux of CO_2 between the biosphere and atmosphere (Baldocchi, 2020). Since the late 1990s, global networks of EC towers (e.g. FLUXNET, AmeriFlux, AsiaFlux, etc.) have accumulated long time series of carbon and water fluxes from hundreds of sites representing diverse biomes (Baldocchi, 2020). In Europe, the Integrated Carbon Observation System (ICOS) network similarly provides standardized CO_2 flux measurements at dozens of sites. In total, these networks (i.e. about 130 stations across all networks, including 19 ecosystem stations in France) have been invaluable for linking ecosystem carbon exchange to climate drivers. These networks include sites across continents (North America, Europe, Asia, Africa, etc.) and ecosystem

https://doi.org/10.5194/egusphere-2026-524
Preprint. Discussion started: 10 February 2026

types from boreal and temperate forests to grasslands, croplands, wetlands, and even urban landscapes. For example, Baldocchi (2020) notes that EC networks now span the main climate and ecological spaces, revealing how GPP and ecosystem respiration respond to sunlight, temperature and moisture. These multi-decadal observations have elucidated several key environmental controls on ecosystem carbon cycling. Solar radiation emerges as the primary driver of photosynthetic carbon uptake, with light response curves showing saturation effects at high irradiance levels and demonstrating how different vegetation types exhibit varying light-use efficiencies (Reichstein et al., 2007; Wohlfahrt and Gu, 2015). Temperature controls operate through multiple pathways: while moderate warming generally enhances both photosynthesis and respiration, the temperature sensitivity (Q_{10}) of respiration typically exceeds that of photosynthesis, leading to reduced net carbon uptake at higher temperatures (Lloyd and Taylor, 1994; Mahecha et al., 2010). Moisture availability represents another fundamental control, with VPD strongly regulating stomatal conductance and thus photosynthetic rates, while soil water content directly affects both plant productivity and microbial respiration (Knauer et al., 2018; Novick et al., 2016).

EC measurements also have well-known limitations; for instance, raw flux time series typically contain gaps due to instrument maintenance, metrological conditions (precipitation), low turbulence or filtering of spurious data. Then, filling these gaps is necessary, requiring statistical or machine-learning gap-filling routines, which can at the same time, introduce uncertainty if large or systematic gaps occur (Gao et al., 2023). Moreover, an EC tower integrates fluxes over an upwind footprint whose size and shape change with surface roughness, atmospheric stability and wind direction; in heterogeneous landscapes a single tower may sample multiple land covers, complicating attribution of fluxes to specific fields or vegetation types. Such footprint heterogeneity can bias estimates when land cover is patchy, a particular concern for small agricultural fields in a mosaic of crops and fallows (Kumari et al., 2020a; Bou-Zeid et al., 2020).

Recently, Machine Learning (ML) techniques have been increasingly applied to model and gap-fill carbon fluxes, taking advantage of large EC datasets and remote-sensing/meteorological inputs. Unlike simple empirical regressions or process-based models that require detailed parameterization, ML methods can capture complex nonlinear interactions without explicit mechanistic assumptions. Typical algorithms include Random Forests (RF), artificial neural networks, support vector machines, and ensemble approaches. For example, Zeng et al. (2020) used a RF model to upscale EC-based net ecosystem exchange (NEE), gross primary production (GPP) and community respiration (CR) from FLUXNET datasets across the globe, producing high-resolution carbon flux maps. In agricultural contexts, ML has proven effective for both gap-filling and predictive modelling. Gao et al. (2023) demonstrated that an RF-based gap-filling framework (combined with moving-average decomposition) outperformed conventional methods (including linear interpolation, mean diurnal variation, and look-up table approaches commonly used in the FLUXNET standardized processing) over extended CO_2 flux gaps. A recent study applied a knowledge-guided ML framework to agroecosystems in the U.S. Corn Belt and showed it surpassed both pure process models and “black-box” ML models in quantifying carbon dynamics (Liu et al., 2024). These studies highlight key advantages of ML, i.e., flexibility in assimilating diverse inputs (weather, soil moisture, phenology, management) and the ability to identify subtle

https://doi.org/10.5194/egusphere-2026-524
Preprint. Discussion started: 10 February 2026

patterns in flux variability. In practice, Random Forests are especially popular for flux prediction because they are robust to overfitting and provide variable importance metrics.

In this context, the La Rochelle Zero Carbon Territory (LRTZC) project (2019-2027) provides a regional framework for carbon monitoring and mitigation in the perimeter of La Rochelle Agglomeration. The project has pledged carbon neutrality by 2040 through combined mitigation and sequestration efforts. Under LRTZC, the Blue Carbon axis and associated research actions target carbon fluxes in coastal ("blue carbon") and retro-littoral ecosystems. As part of these efforts, an Eddy Covariance flux tower has been established from February 2023 to February 2024 in a rural wetland (freshwater marsh, Marans) to monitor retro-littoral atmospheric CO_2 exchanges. This wetland ecosystem is constituted by agricultural parcels (terrestrial compartment) separated by ditches (aquatic compartment). Because the EC system cannot fully isolate fluxes from the water ditches, this single tower overlooks three adjacent fields with different crops and management histories. By partitioning the 360° EC data into specific chosen wind-direction sectors, the "wind-sector approach" adopted in the present study allows analysing separate NEE time series for each parcel of interest depending on wind directions.

The objective of this study was to estimate the carbon budgets of the three individual fields using the sector-specific EC data. Random Forest models were built for each wind sector to predict CO_2 flux from meteorological and soil variables measured at the tower. Annual NEE was then computed for each parcel. Diurnal flux dynamic was also examined to distinguish photosynthetic uptake from nighttime respiration and thus quantify the contribution of respiration to each parcel's carbon budget. To test the benefit of this disaggregated approach, a "pooled" model was also trained using all data from all sectors (ignoring field boundaries), and its flux predictions and budget were compared to those from the separate specific models. The hypothesis was that sector-specific models would more accurately capture each field's distinct CO_2 exchange (reflecting crop and management differences) and thus yield more precise carbon budgets than a single model that pooled all fields. By evaluating disaggregated versus pooled modelling, the study aimed to demonstrate how wind-sector partitioning could enhance carbon monitoring in heterogeneous agricultural landscapes. In this way, complete annual carbon budgets of neighbouring fields could be compared under the same climatic conditions without multiple tower needs.

2 Materials and methods

2.1 Study site

The study was conducted in the city of Marans, located in the Charente-Maritime department in southwestern France (46.31° N, 0.99° W). Charente-Maritime is characterized by a temperate oceanic climate and a predominantly agricultural landscape, with 62% of its surface area spent to agricultural use, amounting to 425,267 ha (Agreste, 2020). The regional land use is dominated by cereal crops (63% of the utilised agricultural area, UAA), followed by permanent grasslands (18%), alongside viticulture and livestock farming (Agreste, 2020).

https://doi.org/10.5194/egusphere-2026-524
Preprint. Discussion started: 10 February 2026

The experimental site comprises three adjacent land parcels representative of the regional land use structure. To the northeast, a parcel was cultivated with mixed grain, sown in autumn and harvested on 24 May 2023, after which the field remained as bare soil for the remainder of the measurement period. To the south, a second parcel was planted with wheat in February and harvested on 10 July 2023. In the northwest, a permanent grassland parcel, continuously grazed by cattle from June to November, was maintained throughout the study. Each parcel is delineated by hydrological features, including a network of drainage ditches typical of the Marais Poitevin wetland system (Butzer, 2002). The Brune Ditch runs between the northern parcels and the wheat parcel and is intersected by a smaller secondary ditch bordered by sparse woody vegetation separating the mixed grain and grassland fields.

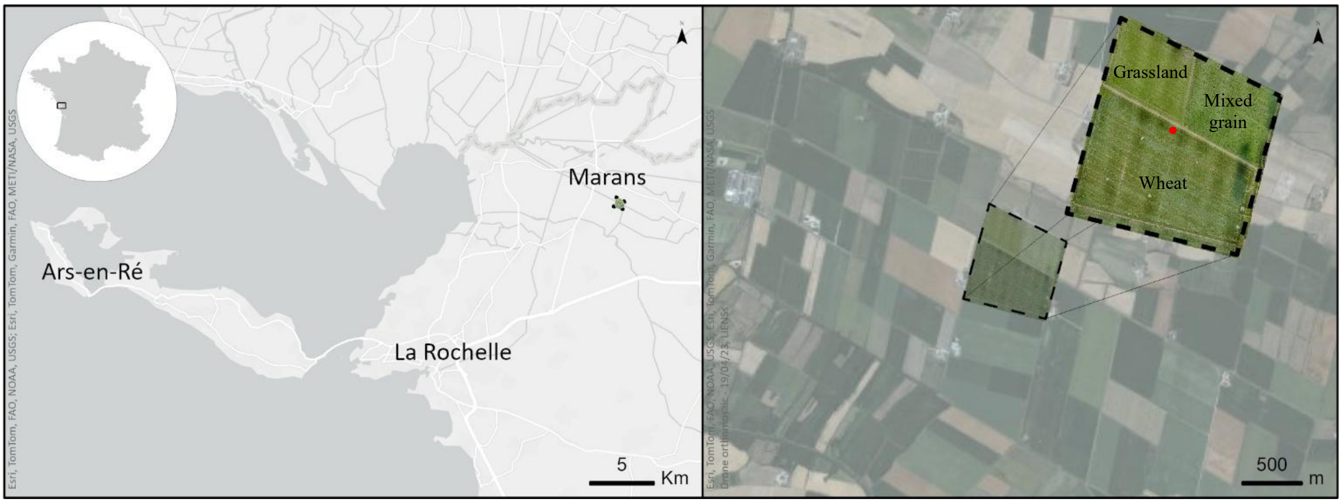

Figure 1. Agricultural fields located in the Poitevin Marsh (Marans city) seen by the atmospheric Eddy Covariance station (red dot) deployed from February 2023 to April 2024. Wheat field in the south, mixed-grain field in the northeast and grassland in the northwest sectors (Drone orthomosaic image taken in February 2023). The Brune Ditch (in brown) orientated from west to east, separates wheat fields in the south from mixed-grain and grassland fields in the north.

The Eddy Covariance (EC) tower was installed on the 1st of February 2023 a narrow-grassed strip approx. 5 m wide adjacent to the Brune Ditch, providing a central location from which flux measurements could be made across the multiple land covers. The site configuration allowed for the assessment of atmospheric CO_2 fluxes across contrasting land uses within a complex agricultural landscape.

2.2 Atmospheric CO_2 exchanges and associated meteorological data measured at the ecosystem scale by Eddy Covariance method

2.2.1 Eddy Covariance data acquisition

The atmospheric Eddy Covariance technique is a micrometeorological method that quantifies net CO_2 fluxes at the ecosystem-atmosphere interface. In the atmosphere, CO_2 is transported by numerous homogeneous eddies of varying size and frequency. These eddies are in the surface boundary layer. This method relies on capturing, within these eddies, the covariance

https://doi.org/10.5194/egusphere-2026-524
Preprint. Discussion started: 10 February 2026

between vertical wind speed (w), air density (ρ), and the dry mole fraction of the gas of interest (s), which can be expressed as:

$$F = \overline{\rho w s} \approx \overline{\rho w' s'}$$

where the overbar indicates the time averaging and the prime represents fluctuations around this average (Burba, 2013; Reynolds, 1886). In this study, measured fluxes were averaged every 10 minutes to maximize the number of observations. Negative CO_2 fluxes indicate the ecosystem acts as a CO_2 sink, while positive fluxes indicate ecosystem source behaviour. Fluxes are given in µmol m^{-2} s^{-1}.

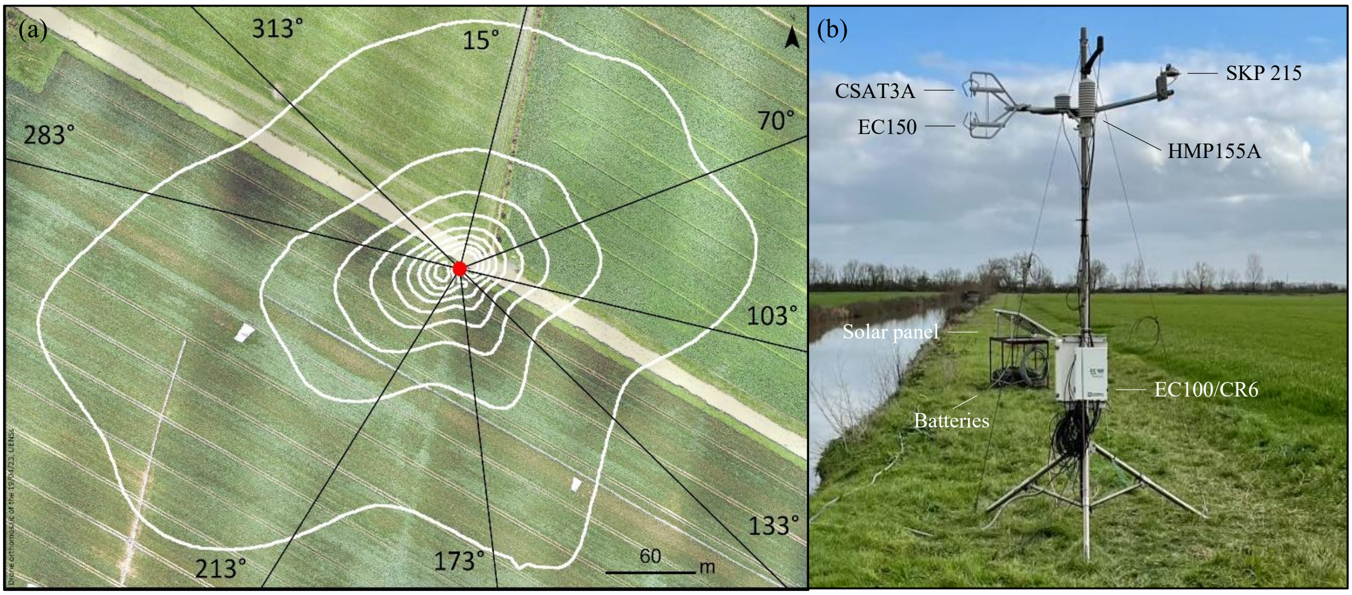

Figure 2. (a) Study site spatial partitioning into wind direction sectors for footprint-based attribution of CO_2 flux measurements to land cover types. High-resolution drone orthomosaic of the study area showing angular sectors centred on the Eddy Covariance (EC) tower (red dot). 15° to 70°: hybrid part of the site, 70° to 103°: mixed grain, 133° to 283° (excluding 173° to 213°, see main text explanations): wheat and 313° to 15°: grassland. 10% to 90% contour lines in white of the annual footprint. (b) The atmospheric EC station set-up with the two main anemometer and CO_2 EC sensors (CSAT3A and EC150, Campbell Sci.) linked to EC100 electronics module connected to the data acquisition central (CR6), with the associated environmental sensors (HMP155A, SKP 215 and TE525MM). The system is powered by batteries charged by solar panels (see main text for more details).

EC station (Campbellsci), installed and monitored from February, 1st 2023 to April, 3rd 2024 between 3 agricultural parcels (Fig. 1), includes several key sensors positioned at the top of a 3m tower mast (Fig. 2b). These sensors include an ultrasonic anemometer (CSAT3A) that measures three-dimensional wind speed components, and an open-path IRGA (EC150, connected to the EC100 central) that measures CO_2 and H_2O concentrations in the air both at a frequency of 20 Hz. The tower is also composed of additional sensors measuring various environmental parameters every 10 minutes: a photosynthetically active radiation (PAR) sensor (SKP215), an air temperature and relative humidity sensor (HMP155A), and a rainfall sensor (TE525MM, Texas Electronics). Soil temperature and water content were measured by another probe (CS655). The data

https://doi.org/10.5194/egusphere-2026-524
Preprint. Discussion started: 10 February 2026

acquisition system was powered by two batteries (12 volts, 260 Ah) charged by monocrystalline solar panels (24 V, 200Wp module with MPPT 100 V/30 A controller; Victron Energy). High-frequency data were recorded on an SD micro-card and replaced every two weeks along sensor cleaning. Meteorological data were stored in the central acquisition system (CR6 datalogger, Campbellsci) (Fig. 2b).

2.2.2 EC data processing and filtering

Raw EC data were processed using the EddyPro software (EddyPro® v7.0.8, LI-COR Inc.) to ensure accurate CO_2 flux measurements. Following Vickers and Mahrt (1997) the processing included several key steps: (1) unit conversion to check that the units for instantaneous data are appropriate and consistent to avoid any errors in the calculation and correction of CO_2 fluxes; (2) despiking to remove outliers in the instantaneous data from the anemometer and gas analyser due to electronic and physical noise and replaced the detected spikes with a linear interpolation of the neighbouring values; (3) amplitude resolution to identify situations in which the signal variance is too low with respect to the instrumental resolution; (4) double coordinate rotation to align the x axis of the anemometer to the current mean streamlines, nullifying the vertical and cross-wind components; (5) time delay removal by detecting discontinuities and time shifts in the signal acquisition from the anemometer and gas analyser; (6) detrending with removal of short-term linear trends to suppress the impact of low-frequency air movements; and (7) performing the Webb-Pearman-Leuning (WPL) correction to take into account the effects of temperature and water vapor fluctuations on the measured fluctuations in the CO_2 and H_2O densities (Burba, 2013). CO_2 fluxes were calculated using the linear detrending method (Gash and Culf, 1996) and averaged over 10-minute intervals. Data with more than 10% missing high-frequency data over these 10-minutes were excluded. Then, EddyPro software outputs contains 4% missing values. Additionally, some extreme values in data were identified and removed using the median absolute deviation (MAD) method (Papale et al., 2006). The MAD was calculated over a 2-week window separating daytime and night-time periods. Data above 5.2×MAD were removed. Without extreme values, the number of missing values reaches 12% for the studied period from 2023-02-01 to 2024-01-31. Finally, data were filtered removing periods where friction velocity (u^*) values were less than 0.1 m s^{-1}. This parameter quantifies atmospheric turbulence then it allows identifying poorly mixed periods. The EC method often underestimates fluxes during these stable periods due to insufficient turbulent mixing. During these periods, the near-ground air can be decoupled from the air above, leading to an accumulation of CO_2 that is not exactly captured by measuring instruments (Barr et al., 2013; Gu et al., 2005). This u^* filter optimizes the accuracy of EC measurements particularly during night. After this last filtration the data set contains a total of 32% missing values with 23% of filtered data corresponding to the night, compared with 9% during the day. For more detail, see for instance Mayen et al. (2024) and (2025).

https://doi.org/10.5194/egusphere-2026-524
Preprint. Discussion started: 10 February 2026

2.3 Intermittent EC data modelling

2.3.1 Landscape-based wind sector classification around the EC tower

To spatially constrain the surface sources contributing to the measured CO_2 fluxes, we delineated a set of wind sectors that reflect both the surrounding land-cover distribution (Fig. 2a) and the roughness-related flow heterogeneity inferred from turbulence measurements (Fig. 3). In addition to the spatial analysis of landscape structure, we used the ratio between friction velocity (u^*) and mean wind speed (U) as a function of wind direction. Because u^* responds sensitively to upwind vegetation height, discontinuities and surface roughness, directional variations in the u^*/U ratio provide an empirical signature of surface-roughness transitions, making it possible to identify, the position of ditch banks, riparian vegetation or flow disturbances induced by the tower infrastructure. This approach was particularly effective after mowing, when all cropped fields were essentially bare soil while riparian corridors remained vegetated, thereby amplifying roughness contrasts between parcels and allowing a precise alignment between directional u^*/U features and landscape elements.

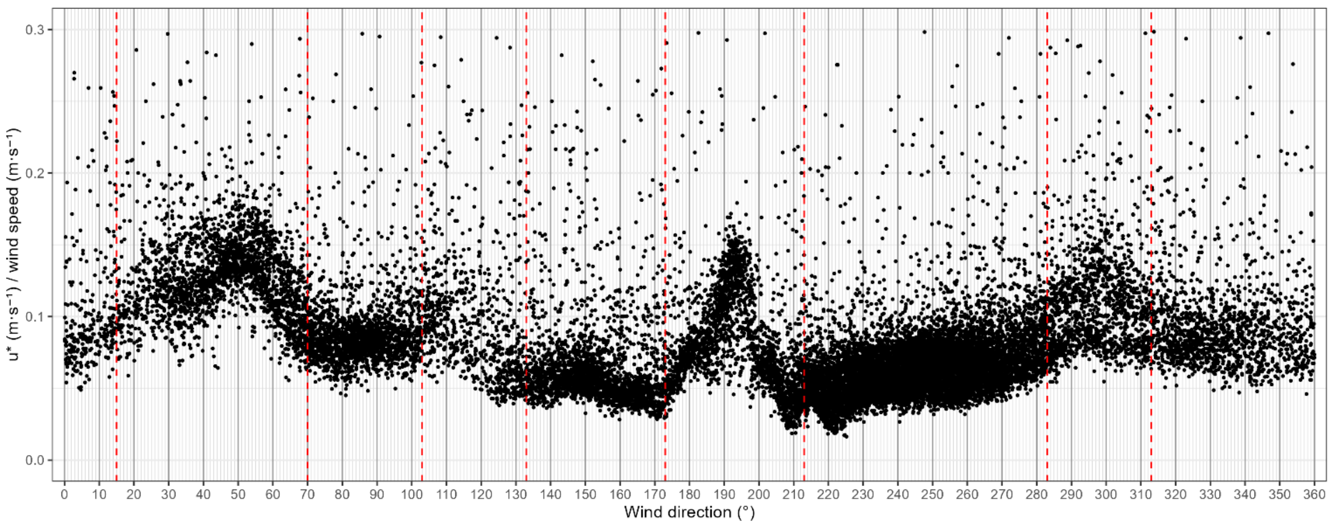

Figure 3. Directional variability of the u^*/U ratio after wheat harvest (10/07/2023), highlighting roughness transitions and disturbances used to define wind-sector boundaries around the EC tower.

Based on the combined interpretation of land-cover maps and directional u^*/U patterns, we redefined the sector boundaries to isolate homogeneous source areas and exclude directions affected by ditches or wake effects. The hybrid sector was set between 15° and 70°, covering the transition zone between grassland and mixed-grain parcels together with associated riparian vegetation. The mixed-grain sector extended from 70° to 103°, up to the first ditch axis, whose influence became evident in the u^*/U signal; directions between 103° and 133° were therefore removed to avoid contributions from the riparian corridor bordering the ditch. The wheat field formed a broad upwind domain from 133° to 283°, within which a directional interval (173-213°) was excluded since it corresponds to the sonic-anemometer wake, whose peak is clearly visible at 193° (Fig. 3). Although the wake does not bias CO_2 fluxes directly, it alters u^* in such a way that the standard u^* filter (< 0.1 m s^{-1}) becomes

https://doi.org/10.5194/egusphere-2026-524
Preprint. Discussion started: 10 February 2026

unreliable; removing ±20° around the wake peak ensured the validity of the filtering procedure while preserving a sufficiently large wheat-sector dataset. Finally, the second ditch sector (283-313°), centred around the opposite ditch axis (~298°), was also excluded using a ±15° margin derived from its roughness signature, for the same reasons as the first ditch interval, namely, to avoid flux contributions from riparian vegetation lining the ditch. The permanent grassland was assigned to the 313-15° sector, covering the pasture area while avoiding adjacent riparian strips. Together, these updated sector boundaries (Figs. 2a and 3) provide a spatially coherent partitioning of the landscape surrounding the EC tower that accounts for surface-roughness transitions and ensures that each retained sector corresponds to a homogeneous and well-defined source area for CO_2 flux interpretation. As a result of this sectorization, only 39% of the available flux data were retained for subsequent analyses.

The Brune ditch sector was not considered due to its narrow width, which prevents obtaining sufficiently representative 10-minute fluxes. The EC technique relies on the averaging of high-frequency turbulent fluxes over discrete time intervals (typically 10-30 min). Within such intervals, both wind direction and speed can considerably fluctuate, meaning that the mean wind direction does not strictly correspond to a fixed upwind source area. As a result, each 10-minute flux integrates signals from multiple surfaces whose relative contribution varies with atmospheric stability, turbulence intensity, and surface roughness. Previous footprint analyses have shown that a significant fraction of the measured fluxes (>75% of flux contributions) are generally confined within upwind distances between 15 and 20 times the measurement height, disputing the applicability of the traditional "1:100" fetch-to-height rule under unstable conditions (Kumari et al., 2020). In the present case, this implies that even small fluctuations in wind direction can cause the footprint to intermittently include or exclude the ditch and its riparian margins, preventing any reliable isolation of ditch fluxes within a single directional sector.

Given its narrow width of approximately 12 m, the Brune ditch represents only a minute fraction of this footprint and cannot generate a dominant or isolable signal within the turbulent flow. Moreover, the ditch is not aligned with the main axis of the EC tower, making it geometrically impossible to define a wind sector that would exclusively sample fluxes from its surface. Any such sector would inevitably include contributions from adjacent vegetation and soil surfaces, especially from the riparian strip bordering the ditch.

This targeted sector classification enables a more precise attribution of measured CO_2 fluxes to discrete land cover types, while acknowledging the heterogeneity of real-world agricultural mosaics. By isolating homogeneous land parcels and minimizing contamination from unmanaged or mixed areas, this approach improves the interpretability of flux measurements in the context of landscape-scale carbon dynamics.

2.3.2 Modelling Scenarios and Sector-Specific Approach

To complete and fully characterize the spatio-temporal dynamics of the Net Ecosystem Exchange (NEE) measured by EC over the February 2023 - February 2024 period across the study site, Random Forest (RF) models were implemented according

https://doi.org/10.5194/egusphere-2026-524
Preprint. Discussion started: 10 February 2026

to two distinct strategies. In the first strategy, Scenario 1, involved training a single global RF model using pooled data from all sectors. This global model was intended to serve as a baseline for comparison, assessing whether joint modelling could match or outperform sector-specific models.

In parallel, an alternative approach (Scenario 2) separate RF models were trained for each landscape-based wind sector classification area and key temporal subdivision, accounting for phenological shifts such as crop harvest for instance that influence flux dynamics over the wheat and mixed-grained areas. Specifically, for each crop parcel, pre- and post-harvest periods were modelled independently to better capture ecosystem transitions, resulting in seven sector-specific models overall (Table 1). Both strategies used the same explanatory variables described in Section 2.3.3 to ensure comparability and comparison.

Table 1. Number of observations recorded each 10 minutes from 01/02/2023 to 31/01/2024 for each selected land cover type (see Fig. 2 and main text for details) and percentage of observations relative to the total number of measurements over the entire year in parentheses. Before and after representing pre- and post- harvest measurements. Harvesting occurred on May 24 for mixed grain and on July 7 for wheat.

Hybrid		Mixed grain		Wheat		Grassland
Before	After	Before	After	Before	After	
2380 (4%)	2101 (4%)	832 (2%)	1533 (3%)	4685 (9%)	6666 (13%)	2192 (4%)

2.3.3 Selection variables for Random Forest modelling

Although variable selection procedures such as Variable Selection Using Random Forest (VSURF) (Genuer et al., 2010) are commonly used to reduce dimensionality prior to Random Forest modelling, we did not apply automated selection in this study. Instead, we opted for a targeted set of explanatory variables a priori chosen based on their established mechanistic links with CO_2 fluxes and their relevance in surface-atmosphere exchange studies. All models were therefore trained using the same set of predictors: photosynthetically active radiation (PAR), day of year (DOY), a qualitative day-night indicator, relative air humidity, soil moisture, soil temperature, wind direction, and air temperature. PAR directly regulates photosynthetic activity and light-driven variations in ecosystem CO_2 uptake; DOY captures seasonal changes in vegetation state and radiation regime; the day-night indicator separates radiative and non-radiative control periods, which exhibit contrasting drivers of respiration and assimilation. Relative humidity and air temperature influence stomatal conductance and microbial respiration, while soil moisture and soil temperature jointly modulate below-ground respiration and substrate availability. Wind direction was included to account for directional heterogeneity in source areas. Importances of these variables for each model are provided in the Appendix A. This expert-driven approach ensured that all major biophysical drivers of CO_2 exchange were represented while maintaining comparability across sectors and modelling exercises.

https://doi.org/10.5194/egusphere-2026-524
Preprint. Discussion started: 10 February 2026

2.3.4 Model evaluation and hyperparameter optimization

To ensure rigorous model optimization and performance evaluation, a systematic approach was implemented. The Random Forest hyperparameter optimization specifically focused on tuning the number of predictors sampled for splitting at each node (mtry), while the number of trees (ntree) was fixed at 400 based on preliminary analyses showing performance stabilization beyond this threshold (Breiman, 2001). The mtry parameter was optimized using a sequential grid search approach, testing values from 1 to the total number of selected predictors. For each mtry value, a Random Forest model was trained on the selected variables, and the out-of-bag (OOB) error from the final tree (ntree = 400) was recorded as the performance metric. The optimal mtry value was selected as the one yielding the lowest OOB error.

Once optimized, model performance was robustly evaluated for both modelling scenarios. In Scenario 1, the global model was trained using the optimal mtry value and evaluated independently for each sector by computing Bias, RMSE, and R^2 metrics on sector-specific subsets of the data. In Scenario 2, separate sector-specific models underwent their own mtry optimization following the same protocol, with each sector's optimal mtry determined independently based on minimizing OOB error.

This streamlined optimization approach leveraged the inherent cross-validation properties of Random Forest's OOB error estimation, eliminating the need for additional train/test splitting while ensuring robust hyperparameter selection. Finally, each model (global or sector-specific) was trained on the full corresponding dataset using the optimal mtry and ntree = 400 before being used for final CO_2 flux predictions. This evaluation framework-maintained consistency while allowing direct comparison between sector-specific and global modelling strategies.

2.4 Cumulative Net Ecosystem Exchange estimations

Annual carbon budgets were estimated for each parcel using the predicted CO_2 fluxes from both the global and crop-specific models. Predictions were made at 10-minute intervals and expressed in µmol CO_2 m^{-2} s^{-1}. Cumulative annual fluxes were obtained by summing all predicted values for each parcel and converting the total to grams of carbon per square meter per year (gC m^{-2} yr^{-1}) using a factor of 0.0072.

To distinguish carbon balance components, fluxes were separated into daytime and nighttime subsets. Daytime period (NEE_{day}) EC data were assumed to reflect gross primary production (GPP) though no Kowalski et al. (2003) partition was attempted due to wind direction change with different corresponding habitats seen by the EC tower during each day; nighttime fluxes (NEE_{night}) were attributed to ecosystem respiration (Reco). Separate cumulative sums were computed for each period, enabling quantification of both photosynthetic uptake (NEE_{day}) and respiratory release (NEE_{night}).

https://doi.org/10.5194/egusphere-2026-524
Preprint. Discussion started: 10 February 2026

These partitioning estimates provided a more detailed understanding of metabolic fluxes and processes, allowing for the decomposition of net annual balances into their physiological components. The outputs also enabled a direct comparison between the two modelling strategies, assessing the consistency of carbon budget estimations across different levels of model complexity.

3 Results

3.1 Performance of the global and sector-specific Random Forest models

To assess the predictive accuracy of the Random Forest (RF) approach for the different agricultural land covers monitored at the studied site, two modelling strategies were evaluated, a global model trained on the entire dataset, taking vegetation type into account only through a qualitative variable (Scenario 1), and crop-specific models trained independently for each land cover type (Scenario 2).

For all land cover types, performance differences between the global and crop-specific models were minimal (Fig. 5 and 6). For most crops, R^2 values were almost identical between both scenarios and consistently high, indicating robust predictive performance whatever the modelling strategy. For example, for permanent grassland, both models achieved an R^2 of 0.86. Similarly, in pre-harvest hybrid crop plots, R^2 values were 0.92. RMSE and bias measurements followed the same trend, with only marginal differences between both approaches. However, a notable exception was observed for post-harvest wheat plots. In both modelling scenarios, predictive performance dropped, with R^2 values at 0.44 for both scenarios. This reduced accuracy may reflect greater complexity or noise in the post-harvest flux signals, potentially due to signal disruption from the November storm which introduced a strong rainfall event (visible in Figure 4e) and field inundation during several days as observed at this period; in turn it likely generated artificial flux variations not linked to actual plant or soil activity. Another consistent observation in both scenarios was a greater dispersion of prediction errors for wheat plots, both pre- and post-harvest. In the scatter plots, these plots showed greater variance and a tendency to deviate from the 1:1 line, particularly under low flux conditions. This suggests either a higher degree of temporal variability, or unmodeled management practices or events affecting flux behaviour in wheat systems (Fig. 5 and 6).

These limitations are particularly important in the context of sparse measurement periods. For instance, during the spring drought observed in May 2023 (Figure 4c, low humidity, figure 4d, high temperature and figure 4e, low rainfall) which coincided with the mowing period, the lack of available data made it challenging to constrain the model. However, the crop-specific models reproduced the water limitation effect more accurately for wheat and grassland than the global RF model (see Section 3.2), even though these parcels were not harvested during that period.

https://doi.org/10.5194/egusphere-2026-524
Preprint. Discussion started: 10 February 2026

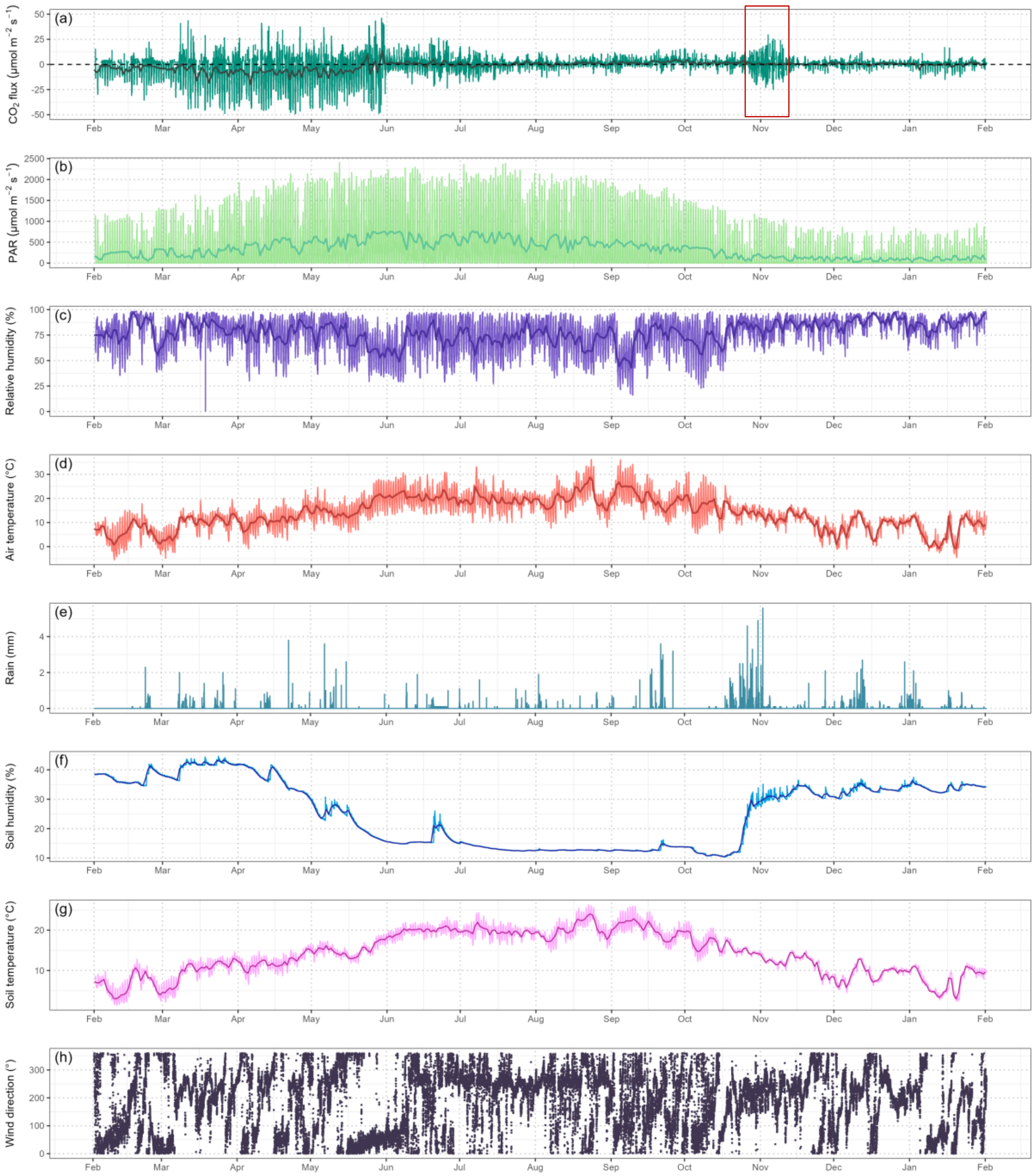

350

Figure 4. Atmospheric Eddy Covariance measured time series from 01 February 2023 to 31 January 2024 of (a.) atmospheric CO_2 exchanges, (b.) Photosynthetically Active Radiation (PAR), (c.) relative humidity, (d.) air temperature, (e.) rain, (f.) soil humidity, (g.) soil temperature and (h) wind direction. For CO_2 fluxes, PAR, relative humidity, air temperature, soil humidity and soil temperature, the continuous line represents the daily average obtained from the 10 min values. Box in red November's storm.

355

https://doi.org/10.5194/egusphere-2026-524
Preprint. Discussion started: 10 February 2026

3.2 Flux dynamics across land cover types

While overall predictive metrics (R^2, RMSE, bias) appeared similar between the global and sector-specific models (Section 3.1), a detailed analysis of the temporal dynamics of CO_2 fluxes reveals a clear advantage of the crop-specific approach (Scenario 2).

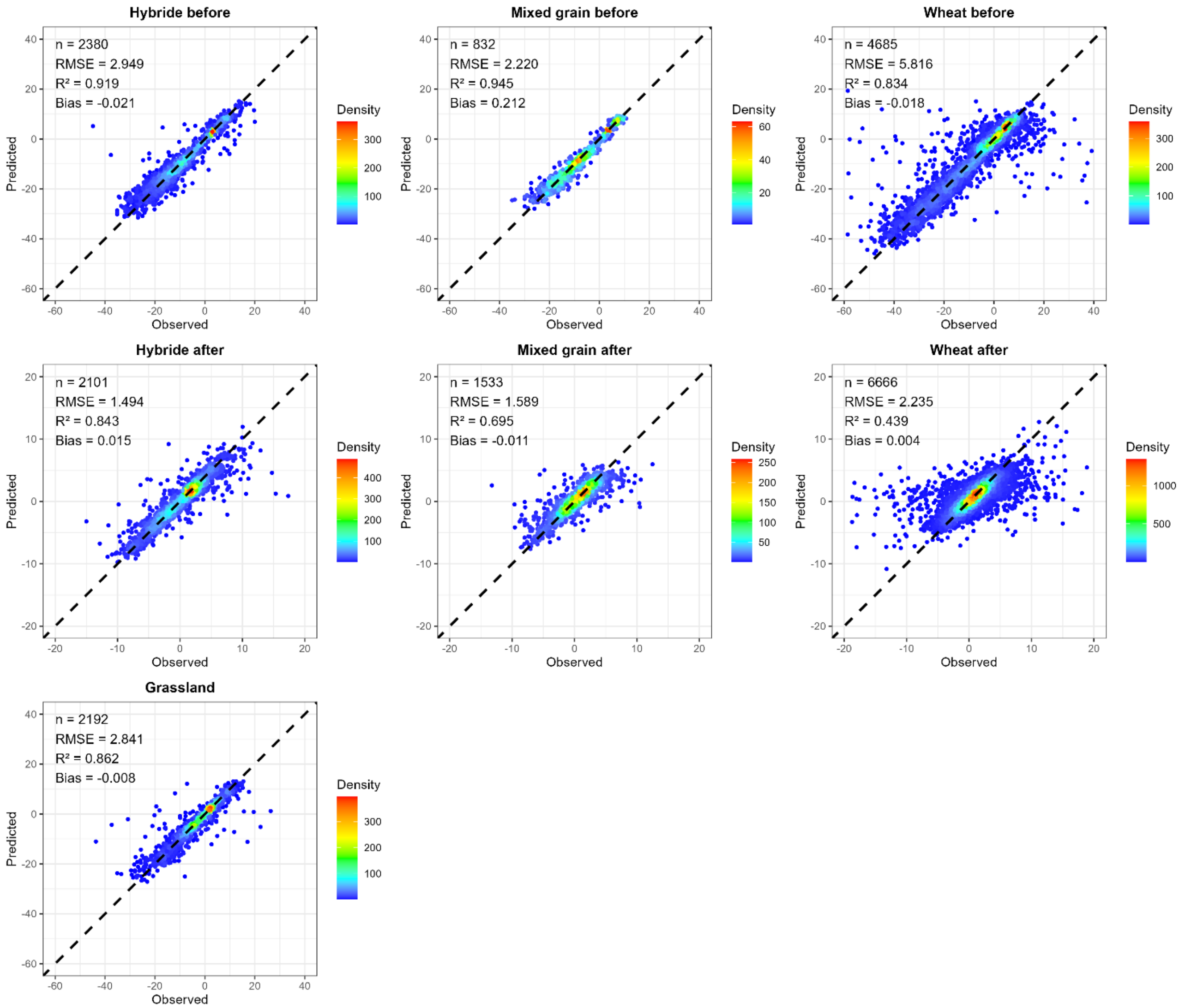

Figure 5. Comparison between measured and predicted CO_2 fluxes for each specific land cover type on the test datasets using the global Random Forest model (Scenario 1). Predictions were made using a single model trained on the full dataset. Mean performance metrics (Bias, RMSE, R^2) are reported for each panel. Colour scale represents the point density, warmer colours indicating higher concentration of data points. Before and after referring, respectively, to the pre- and post- harvest periods. See Table 1 for land cover type description.

Under Scenario 1 (Figure 7), the global model reproduced the broad seasonal trends in carbon fluxes but failed to capture finer-scale temporal variations and parcel-specific dynamics. Predictions exhibited similar patterns across all land cover types,

https://doi.org/10.5194/egusphere-2026-524
Preprint. Discussion started: 10 February 2026

indicating an overgeneralization of flux behaviour. For instance, during the productive phase preceding the harvest in the wheat parcel, the model clearly underestimated carbon uptake, with a maximum measured productivity of -74.78 µmol m^{-2} s^{-1} compared to a maximum predicted productivity of only -34.89 µmol m^{-2} s^{-1}, representing a 46% underestimation. This homogenization contrasts sharply with observed fluxes, which showed that wheat had the highest productivity during that period. A second limitation emerged around the mowing date (24 May 2023). The global model predicted a sharp drop in net carbon uptake simultaneously across all parcels. However, this abrupt decline was only observed in the hybrid and mixed grain parcels, where management events took place. In the wheat parcel, a decrease in productivity was observed as well, but was more gradual and not linked to mowing but to a drought event clearly visible in the environmental time series (Figure 4e, low rainfall and 4f, reduced soil moisture), as well as to the natural wheat cycle and its senescence phase, during which the crop becomes less productive. In consequence, the global model failed to distinguish these drivers and instead introduced a synchronized shift across all systems. Additionally, a small respiration peak appeared around November in all parcels under Scenario 1, despite it being caused by storm-related noise observed only in the wheat parcel, coinciding with a strong rainfall spike and a sudden increase in soil moisture (Figure 4e and 4f). This artifact, replicated across systems, highlights the model's inability to specifically catch disturbances.

In contrast, Scenario 2 (Figure 8), which relied on crop-specific models, provided a much more accurate and differentiated representation of carbon flux dynamics according to each parcel. In the wheat parcel, the model successfully captured both the intensity of the pre-harvest uptake and the smoother post-harvest decline, closely matching measured values. The sector-specific approach correctly distinguished the less abrupt drop in wheat productivity observed in late May contrarily to the global model trend that produced sharper responses, as those seen in the hybrid and mixed grain systems during their respective harvests on 24th May. For these systems, hybrid and mixed grain flux trends were accurately modelled as rapid declines in uptake following mowing, consistent with field operations. Moreover, the spurious respiration peak observed in Scenario 1 was no longer present in hybrid and mixed grain parcels, confirming that the sector-specific models did not propagate noise originating from unrelated systems. For grassland fluxes, the model reproduced the regrowth phases and moderate seasonal variability typical of unmanaged vegetative cover, improving both the shape and amplitude of predicted fluxes. In grassland, it also successfully reproduced the photosynthetic slowdown during the May drought period (Figure 4), despite of sparse measurements, further highlighting its sensitivity to climatic forcing.

Overall, Scenario 2 outperformed the global model by better capturing observed flux patterns, reducing homogenization effects, and providing more realistic responses to crop-specific phenology and management. However, this improvement was not consistent across all land cover types. In areas with fewer measurements, such as permanent grasslands, model uncertainty remained higher. Moreover, the greater sensitivity of the crop-specific models may also increase the risk of capturing noise or local anomalies. While Scenario 2 marks a clear improvement, it does not fully resolve the challenges of modelling complex agroecosystem fluxes within a wetland terrestrial system and should be further evaluated with independent data.

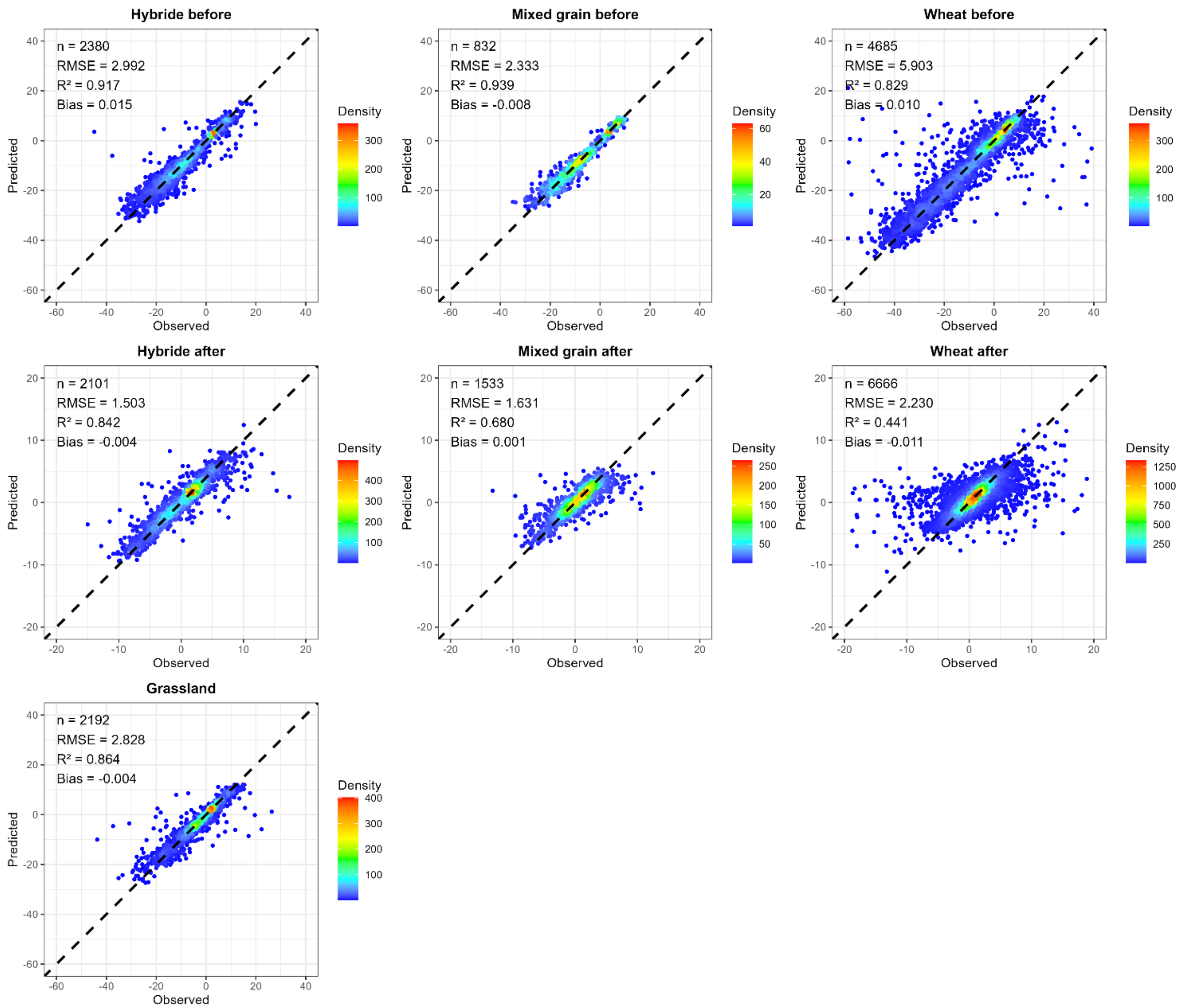

Figure 6. Comparison between measured and predicted CO_2 fluxes on the test datasets using crop-specific Random Forest models (Scenario 2). Each panel presents results from a model trained and tested exclusively on data from the corresponding land cover type. Mean performance metrics (Bias, RMSE, R^2) are reported for each panel. Colour scale represents the point density, warmer colours indicating higher concentration of data points. Before and after referring, respectively, to the pre- and post- harvest periods. See Table 1 for land cover type description.

3.3 Day-night flux partitioning

To further investigate mechanisms underlying net carbon exchange processes and fluxes, total CO_2 fluxes were separated in daytime and nighttime fluxes according to PAR values (Figure 9).

Under Scenario 1 (global model), the cumulative $NEE_{daytime}$ and $NEE_{nightime}$ curves exhibited remarkably similar trends across parcels. $NEE_{daytime}$ curves were nearly indistinguishable throughout the year, with only a slight deviation from the grassland

https://doi.org/10.5194/egusphere-2026-524
Preprint. Discussion started: 10 February 2026

parcel, which ended with the highest $NEE_{daytime}$ value of -813 gC m⁻², compared to -641, -667 and -697 gC m⁻² for mixed grain, wheat and hybrid respectively (Figure 9a). This uniformity mirrors the homogenized flux patterns observed in the time series (Figure 7). $NEE_{nightime}$ curves showed the same convergence, with cumulative values between 595 gC m⁻² (wheat) and 667 gC m⁻² (grassland), except for the hybrid parcel, which showed a slightly higher respiration total of 765 gC m⁻² (Figure 9c).

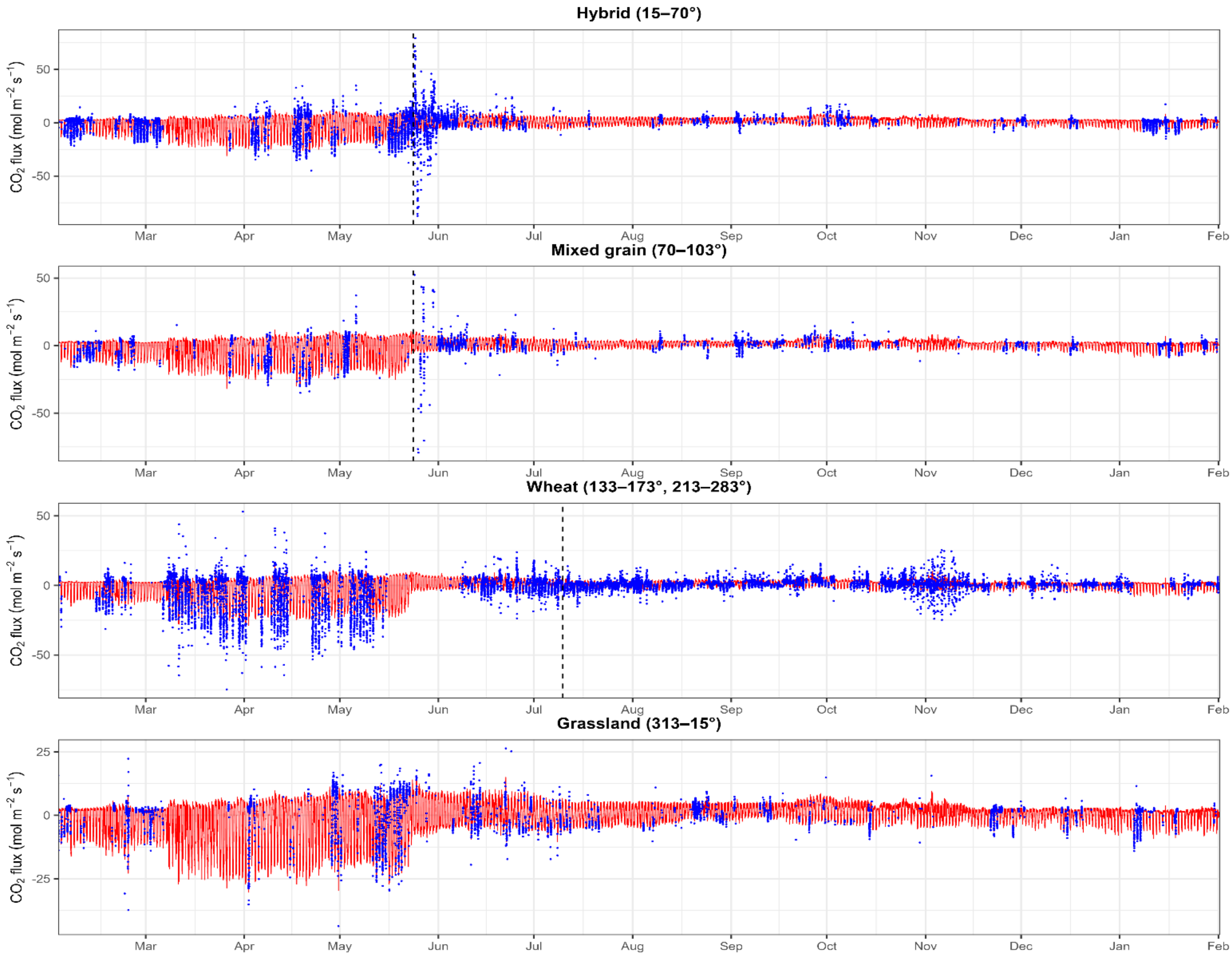

Figure 7. Time series of measured (blue) and predicted (red) CO_2 fluxes using the global Random Forest model (Scenario 1) across land parcels. Dotted lines represent harvests.

In contrast, Scenario 2 (sector-specific models) produced more fine and biogeochemically consistent cumulative flux trends. $NEE_{daytime}$ curves revealed four distinct patterns across the parcels. Notably, the wheat system reached a peak $NEE_{daytime}$ of -844 gC m⁻² at 8th June, reflecting its intense pre-harvest productivity as previously illustrated in the time series (Figure 8). However, following harvest, $NEE_{daytime}$ accumulation slowed down, resulting in a final cumulative value of -764 gC m⁻².

https://doi.org/10.5194/egusphere-2026-524
Preprint. Discussion started: 10 February 2026

Grassland, which was not harvested, maintained modest but continuous photosynthetic activity throughout the year. Despite a lower peak productivity compared to wheat, its persistent growth enabled it to surpass wheat in final $NEE_{daytime}$, reaching -882 gC m^{-2}, the highest $NEE_{daytime}$ value of all parcels. Hybrid and mixed grain systems followed nearly identical $NEE_{daytime}$ trends until harvest date (24th May), after which their curves diverged. The mixed grain parcel reached -431 gC m^{-2}, while the hybrid system continued to accumulate carbon at a reduced rate, ending at -609 gC m^{-2} (Figure 9b). This reflects the model's ability to capture the different post-harvest dynamics of two different systems, contrasts that were not considered under scenario 1. Cumulative $NEE_{nightime}$ under Scenario 2 also revealed more pronounced differences. The hybrid system displayed the highest cumulative respiration (840 gC m^{-2}). The wheat parcel, by contrast, had the lowest $NEE_{nightime}$ (549 gC m^{-2}). Interestingly, the grassland and mixed grain parcels exhibited very similar $NEE_{nightime}$ totals (623 gC m^{-2} and 613 gC m^{-2}, respectively), despite of very different $NEE_{daytime}$ dynamics.

3.4 Annual Carbon Budgets Across Parcels

The net annual carbon budgets, derived from the cumulative sum of predicted daytime ($NEE_{daytime}$) and nighttime ($NEE_{nightime}$) fluxes, provide an integrated view of each parcel's role as a carbon source or sink. These results offer a synthetic outcome of the dynamics presented in previous sections and allow for a direct comparison between the two modelling strategies.

Under Scenario 1 (global model), annual net ecosystem exchange (NEE) cumulative values remained relatively close across all land covers, reflecting the model's tendency to smooth out flux differences due to its pooled training approach. Despite this homogenization, the model still correctly captured the broad source-sink roles of the different systems, consistent with what was given by crop-specific models, but with less contrast. Two groups of parcels emerged: the hybrid and mixed grain systems, which exhibited positive annual NEE cumulative values and thus functioned as net carbon sources, with cumulative totals of +68 gC m^{-2} yr^{-1} and +2 gC m^{-2} yr^{-1}, respectively; and the grassland and wheat systems, which displayed negative NEE values, indicating carbon sink behaviours, with NEE cumulative values of -145 gC m^{-2} yr^{-1} and -72 gC m^{-2} yr^{-1}.

By contrast, Scenario 2 (sector-specific models) produced more contrasted and ecologically coherent annual carbon budgets. The same two functional groups reappeared, but with greater differentiation. The hybrid and mixed grain parcels still acted as carbon sources, with final NEE values rising to +231 gC m^{-2} yr^{-1} and +182 gC m^{-2} yr^{-1}, respectively. The grassland and wheat systems, on the other hand, were both confirmed as net carbon sinks, with highly similar final budgets of -259 gC m^{-2} yr^{-1} and -216 gC m^{-2} yr^{-1}, respectively

https://doi.org/10.5194/egusphere-2026-524
Preprint. Discussion started: 10 February 2026

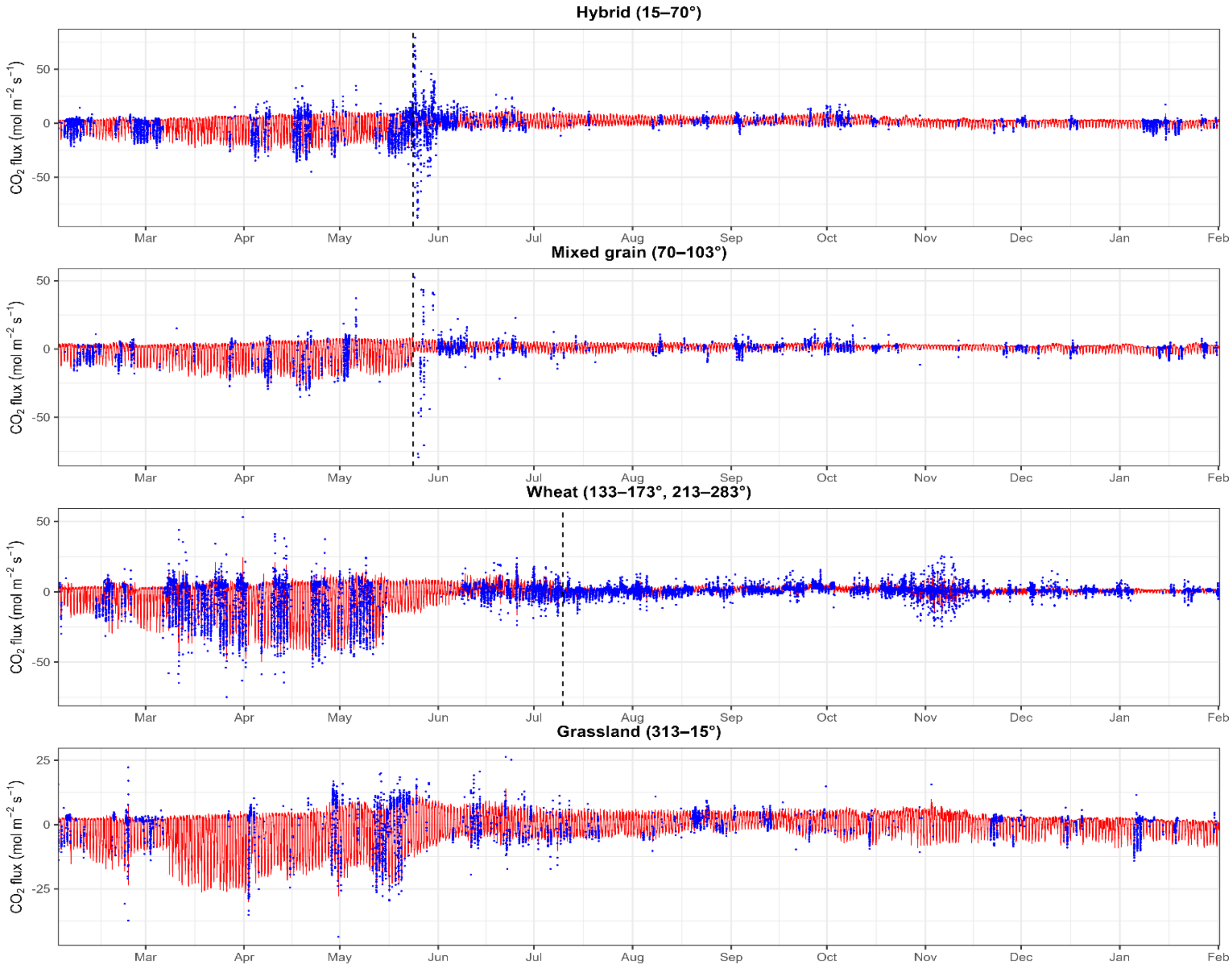

Figure 8. Time series of measured (blue) and predicted (red) CO_2 fluxes using the crop-specific models (Scenario 2). Dotted lines represent harvests.

4 Discussion

4.1 Methodological considerations: single-tower sector partitioning and modelling

Deploying a single Eddy Covariance (EC) tower with wind-sector partitioning enabled the continuous monitoring of multiple adjacent agricultural land covers, representing a cost-effective alternative to multi-tower setups. This approach reduces instrumentation and maintenance costs but inevitably introduces spatial uncertainties in heterogeneous landscapes. The EC flux footprint may encompass several vegetation types depending on wind direction, measurement height, surface roughness, and the stability of atmospheric conditions. Under unstable conditions, the footprint remains narrow and is typically dominated

https://doi.org/10.5194/egusphere-2026-524
Preprint. Discussion started: 10 February 2026

by a single surface type; however, because turbulent exchange is strongest near the tower under such conditions, the relative contribution of nearby elements, such as ditches and riparian vegetation, becomes more pronounced. Conversely, under stable conditions, the footprint expands and integrates fluxes over a larger upwind area, which may include multiple fields and dilute the ditch's influence within the aggregated signal. As demonstrated by Hernandez Rodriguez et al. (2023), such organized heterogeneity can modify observed fluxes by more than 10% compared with a homogeneous land-cover assumption.

In this study, three monitored sectors (grassland, mixed-grain, and hybrid) are directly adjacent to a drainage ditch, whereas the wheat field lies farther away and is unaffected by aquatic surfaces. The ditch and its riparian vegetation contribute additional CO_2 fluxes that cannot be spatially discriminated within the EC footprint. Consequently, fluxes attributed to the grassland, mixed-grain, and hybrid sectors may partly integrate emissions or uptake from the ditch, while the wheat sector provides a purely terrestrial reference. The sector-based strategy therefore associates each flux measurement with the predominant upwind vegetation type (e.g., wheat versus grassland), but this attribution remains imperfect due to the variable footprint geometry. Multi-tower configurations would offer more precise parcel-level discrimination but involve substantial financial and logistical constraints. Hence, the single-tower, wind-sector approach adopted here represents a pragmatic compromise: it enables continuous, multi-cover flux monitoring within a mosaic of agricultural fields and wetland interfaces while accepting a controlled level of footprint mixing and the associated uncertainty.

EC measurements complemented by Random Forest (RF) modelling allowed upscaling and gap-filling of flux data across the different systems, incorporating vegetation-specific and management information. The RF models were robust across land covers, with high performance. However, while global and crop-specific models achieved similar accuracy metrics, their ecological behaviour differed markedly. The global model tended to average flux behaviour across systems, obscuring specific phenological and management-driven variability. For example, it failed to capture the specific productivity phases of each crop and showed muted responses to events such as harvest. In contrast, sector-specific models revealed meaningful ecological patterns and management effects. These models distinguished between gradual, drought-induced NEE declines and the abrupt flux reversals after harvest. They also identified crop-specific daytime ($NEE_{daytime}$) and nighttime ($NEE_{nighttime}$) flux partitioning, accurately reflecting physiological processes. Distinct $NEE_{daytime}$ profiles emerged: wheat showed intense spring uptake that ended abruptly at harvest, grassland showed modest but continuous uptake throughout the season, and the mixed-grain and hybrid systems diverged after May's harvest (the mixed-grain parcel became essentially bare, whereas the hybrid parcel, containing riparian vegetation by the ditch, maintained some photosynthetic activity). These differences mirror results from other studies: for example, Bajgain et al. (2018) found that winter wheat had much higher peak daytime uptake than tallgrass prairie, and that the wheat site became a net carbon source annually whereas the prairie remained a sink. Such nuanced dynamics are essential to understand carbon cycling and management impacts across diverse agroecosystems.

https://doi.org/10.5194/egusphere-2026-524
Preprint. Discussion started: 10 February 2026

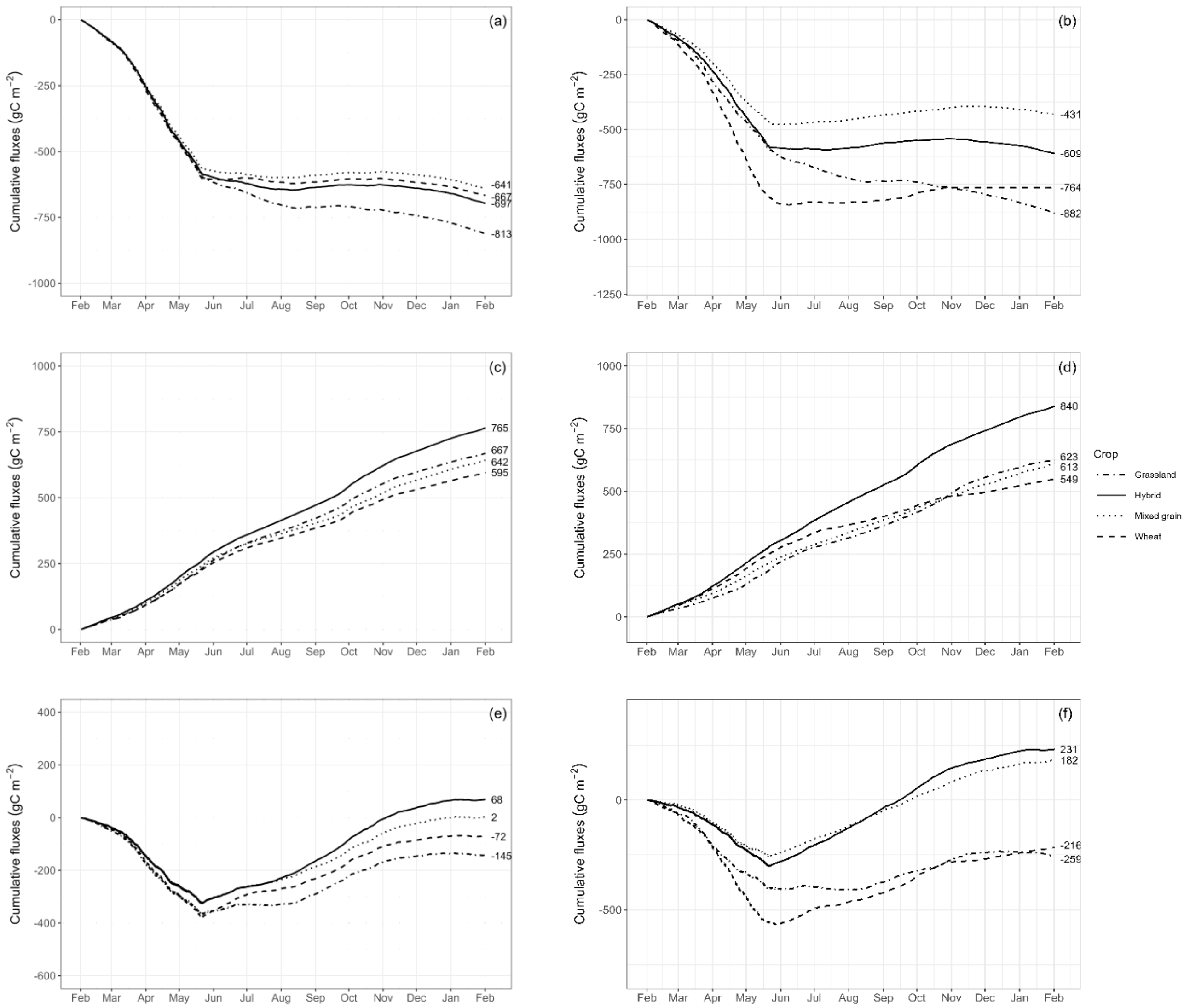

Figure 9. Cumulative CO_2 fluxes by vegetation type and modelling approach, with panels (a), (c), and (e) corresponding to Scenario 1 (global model) and panels (b), (d), and (f) to Scenario 2 (crop-specific models). Panels (a) and (b) represent daytime CO_2 assimilation ($NEE_{daytime}$), panels (c) and (d) nighttime CO_2 emission ($NEE_{nightime}$), and panels (e) and (f) the net cumulative CO_2 exchange. Each curve reflects a specific land cover. Final cumulative values indicate the carbon balance (gC m^{-2} y^{-1}) and the respective contributions of $NEE_{daytime}$ and $NEE_{nightime}$ (gC m^{-2}).

Despite the RF models' overall robustness, performance declined for the wheat sector after harvest. This lower performance does not reflect a fundamental modelling issue, but rather the specific conditions under which the EC measurements were collected during that period. During a series of storms in November, intense rainfall, strong atmospheric turbulence, and rapidly shifting wind directions occurred. During these storm events, the prevailing wind directions caused the EC system to

https://doi.org/10.5194/egusphere-2026-524
Preprint. Discussion started: 10 February 2026

predominantly sample fluxes originating from the wheat sector, even though the disturbance was not specific to that land cover. The combination of precipitation and wind-driven turbulence generated large spikes in the CO_2 signal, leading to spurious flux values that did not represent actual ecosystem exchange. These anomalies were not linked to environmental variability or management practices but instead resulted from temporary disturbances of the measurement system during the storm events. Although part of this noise was removed during preprocessing, some anomalous values could not be fully filtered and therefore remained in the dataset. Consequently, the RF models (both global and sector-specific), which rely on environmental drivers to explain flux variability, were unable to relate these erratic values to any meaningful explanatory variables and failed to reproduce them. In this context, the reduced model performance is not problematic. On the contrary, it indicates that the models do not assimilate or reproduce physically unrealistic fluxes. Importantly, these distorted values were not included in the final predicted time series used for carbon budget calculations. By effectively replacing these anomalies with fluxes consistent with ecologically plausible responses to environmental drivers, the model prevents the propagation of erroneous data and reinforces the reliability of the model-based flux estimates.

To validate the EC-based flux measurements and Random Forest (RF) modelling, static and automated chamber measurements are highly informative. Wang et al. (2013) reported near-identical NEE values using EC and automated chambers in winter wheat, with seasonal EC estimates of -251 gC m^{-2} and chamber-derived values of -205 gC m^{-2}. Similarly, Drewer et al. (2017) found consistent patterns between chamber and EC fluxes in intensively managed grasslands. These studies indicate that chamber measurements can reliably reflect EC fluxes at plot scale and can also capture temporal dynamics (e.g. drought responses or post-harvest changes). Although chamber data have limited spatial coverage, they offer crucial plot-scale insight and could help verify RF model accuracy, especially under flux footprint conditions that are highly localized.

Given the consistently superior performance and ecological coherence of the sector-specific models, all subsequent discussion will focus exclusively on their results.

4.2 Seasonal NEE dynamics: phenological, environmental controls and management

Seasonal patterns of $NEE_{daytime}$ and $NEE_{nighttime}$ varied markedly between land covers and were primarily shaped by phenology, management practices, and environmental constraints. In spring, wheat exhibited the highest rates of daytime CO_2 uptake, with peak productivity in mid-May. This strong early-season sink surpassed that of the grassland, which maintained a more stable but lower carbon uptake throughout the season. These patterns are consistent with findings by Gilmanov et al. (2003), who reported higher gross primary productivity (GPP) in winter cereals compared to temperate grasslands during early phenological stages, due to faster canopy development and higher photosynthetic capacity before senescence or management interventions. For reference, the ditch runs along the mixed-grain, hybrid, and grassland parcels but does not border the wheat parcel, which may partly explain the observed differences.

https://doi.org/10.5194/egusphere-2026-524
Preprint. Discussion started: 10 February 2026

In contrast, the mixed-grain and hybrid sectors initially displayed nearly identical $NEE_{daytime}$ patterns. Prior to the May 24th harvest, both sectors showed similar CO_2 uptake levels, indicating that the hybrid fluxes were dominated by the adjacent mixed-grain plot. After the harvest, however, their dynamics diverged. The mixed-grain sector became essentially bare soil and its daytime sink collapsed, whereas the hybrid sector maintained some photosynthetic activity thanks to the ditch and its riparian vegetation (a strip of grasses and shrubs). This riparian vegetation likely explains why the hybrid sector showed consistently higher $NEE_{nighttime}$ emissions than the pure grassland or mixed-grain sectors, since moist riparian zones are known to sustain elevated respiration due to their higher soil moisture and organic content (Reichstein et al., 2005).

Wheat, on the other hand, transitioned from a carbon sink to a source between mid-May and mid-June as rapid senescence set in. This senescence was likely accelerated by rising temperatures and the onset of drought, making it difficult to distinguish natural maturation from stress responses. At the same time, the grassland experienced gradual reductions in $NEE_{daytime}$, but it never fully ceased assimilation. As a perennial system with only partial grazing (biomass removal by cattle rather than complete mowing), the grassland continued to photosynthesize at a low level even during the driest period. In short, agricultural management drove different flux shifts: the cereal harvest in the mixed-grain parcel caused an abrupt flux reversal, whereas grazing in the grassland produced more moderate, progressive changes. These observations align with Heimsch et al. (2021) and others, who have reported sharper CO_2 flux reversals following harvest compared to grazing in temperate agricultural systems.

The mid-May drought had distinct, asynchronous effects across the systems. In wheat, any drought impact on $NEE_{daytime}$ was largely masked by the overlapping senescence. In the mixed-grain sector, the drought coincided with the interval immediately before harvest; any reduction in uptake was ultimately hard to separate from the imminent harvest removal. By contrast, the grassland showed a clear and sustained reduction in $NEE_{daytime}$ during and after the dry spell, likely due to stomatal closure in response to elevated vapor pressure deficit (VPD). This is consistent with results reported by Flanagan and Adkinson (2011) for temperate grasslands, where water-limiting conditions led to significantly reduced CO_2 uptake.

Across all land covers, the primary environmental drivers of $NEE_{daytime}$ were light (photosynthetically active radiation, PAR), air temperature (T_a) and VPD. Peak CO_2 uptake occurred on sunny, mild days: for example, maximum assimilation occurred at PAR ≈ 1700 μmol m^{-2} s^{-1}, $T_a \approx 22$°C and VPD ≈ 1.2-1.3 kPa (values similar to optimal conditions reported for winter wheat by Wagle et al. (2018). Conversely, hot and dry conditions (high VPD) strongly suppressed photosynthesis and enhanced respiration. Nighttime fluxes remained relatively stable, but $NEE_{nighttime}$ rose modestly with higher temperature and following disturbance events, especially in the hybrid and grassland sectors where plant residues and living vegetation persisted. In particular, the hybrid sector's riparian vegetation and the grassland's residual biomass fuelled elevated microbial and plant respiration at night. These temporal dynamics underscore the tight coupling between phenological development, disturbance regimes and microclimatic conditions in shaping seasonal carbon fluxes in these agroecosystems.

https://doi.org/10.5194/egusphere-2026-524
Preprint. Discussion started: 10 February 2026

4.3 Annual Carbon Budgets of the studied parcels and implications for carbon accounting and limitations

Annual NEE estimates revealed clear contrasts among land uses. The permanently grazed grassland and winter wheat plots acted as strong net carbon sinks (-259 and -216 gC m^{-2} yr^{-1}, respectively), whereas the mixed-grain and hybrid systems were net carbon sources (+182 and +231 gC m^{-2} yr^{-1}). These values are broadly consistent with the literature (Table 2). For example, managed humid grasslands have been reported with annual NEE in the range of roughly -200 to -260 gC m^{-2} yr (Jaksic et al., 2006), and mowed or grazed grasslands often show high seasonal uptake, e.g. Senapati et al. (2014) reported -476 gC m^{-2} yr^{-1} for a mowed grassland and -231 gC m^{-2} yr^{-1} for a grazed grassland. Winter wheat sink strength is also in line with other reported values; for instance, Schmidt et al. (2012) found ∼−270 gC m^{-2} yr^{-1} for winter wheat, through two years of EC measurements.

A key factor underlying these site differences is land-use history. The grassland and wheat plots have been under their respective management for many years, whereas the mixed grain was grassland before measurements year and reverted to grassland afterward (Guignard and Pouponnot, personal communication). Indeed, the mixed-grain system was a one-off cereal rotation rather than an established crop. Crop-rotation studies indicate that continuous annual cropping tends to reduce productivity (and thus carbon uptake) relative to long-term rotations or perennial cover, due to changes in soil structure, nutrient cycling and microbial communities (Liebman and Dyck, 1993). Similarly, biodiversity and rotation experiments have shown that systems with longer-lived, diverse plant communities achieve greater and more stable productivity than single-year crops (Tilman et al., 2006). Then, the modest uptake in the mixed-grain sector likely reflects its transient status: the recent conversion from grassland meant lower soil organic matter quality and microbial efficiency, reducing photosynthetic carbon uptake, while still allowing substantial post-harvest soil respiration.

By contrast, the established winter wheat field behaved almost neutrally in full carbon accounting. Once grain removal (~250 gC m^{-2} via harvest) is considered, our high measured sink would be largely offset. This agrees with other studies of long-term cereal monocultures (e.g. Schmidt et al. 2011), which find that harvest removals can balance the high productivity of wheat. The hybrid system (cereal crop plus adjacent grazed grassland) produced the largest net source. Its amplified emissions arose from both the large respiration pulse of the mixed-grain crop after harvest and the continued nighttime respiration of the perennial grassland component.

The budgets presented here focus solely on atmospheric NEE and harvested biomass, without incorporating all carbon pathways, in particular, changes in soil organic carbon and lateral hydrological fluxes. Simultaneous water pCO_2 measurements conducted in November 2023 within the LRTZC project indicated mean water CO_2 emissions of 12.42 ± 14.54 mmol m^{-2} h^{-1} (equivalent to approximately 3.45 ± 4.04 µmol m^{-2} s^{-1}, data not shown) from the ditch surface that contrast in comparison with cumulated NEE values obtained in the present study; from previous bimonthly water carbon and discharge measurements

https://doi.org/10.5194/egusphere-2026-524
Preprint. Discussion started: 10 February 2026

carried out in 2017 and 2018 in the different watercourses of the Marais poitevin watershed flowing to the Aiguillon bay, an annual terrestrial carbon export of 15 gC m^{-2} yr^{-1} was estimated (Coignot et al., 2020). These carbon fluxes (i.e. water-air CO_2 flux and carbon export values) highlight the importance of lateral aquatic fluxes that need to be taken into account to draw the whole regional carbon budget of the land-sea continuum formed by the Marais poitevin wetland and the Aiguillon tidal bay (Polsenaere, 2025; Polsenaere et al., in prep.).

Table 2. Annual net ecosystem exchange (NEE, in gC m^{-2} yr^{-1}) values found from this study and comparable literature. Site information and methodology are specified. Negative values indicate net uptake (sink). See text for details of site conditions.

Reference (Location)	Vegetation/Crop	Method	Annual NEE (gC m^{-2} yr^{-1})	Notes
Jaksic et al. 2006 (Ireland)	Managed humid grassland	EC (2 years)	-193 (wet year); -258 (dry)	No moisture stress (soil > wilting point)
Senapati et al. 2014 (France)	Sown grassland (mowed)	EC (1 yr)	-476	"Mowing" management; net C storage ~+23 gC (after harvest)
Senapati et al. 2014 (France)	Sown grassland (grazed)	EC (1 yr)	-231	"Grazing" management; net C storage ~+141 gC
Wang et al., 2013 (China)	Winter wheat (crop season)	EC & auto-chamber	-251 (EC, seasonal)	Chamber EC comparison; EC flux matched AC flux within 7%
Schmidt et al. 2012 (Germany)	Winter wheat (annual)	EC (2 yrs)	-270 (Yr1); -270 (Yr2)	High uptake: field was a net source if harvest C removed
This study (France)	Temperate grassland	EC + RF model	-259	Permanent grass; measured 2023
This study (France)	Winter wheat	EC + RF model	-216	Residues removed post-harvest; measured 2023
This study (France)	Mixed grain	EC + RF model	+182	Similar management to wheat, lower growth
This study (France)	Hybrid cereal/grass mix	EC + RF model	+231	Intercropped cereals in riparian buffer

The combined EC-RF framework demonstrates that a single-tower, sector-partitioned approach can yield robust field-scale NEE estimates suitable for integration into regional or national greenhouse gas inventories, particularly in heterogeneous wetland-agricultural environments. By attributing fluxes to discrete land covers, this method bridges the gap between plot-

https://doi.org/10.5194/egusphere-2026-524
Preprint. Discussion started: 10 February 2026

level process studies and coarser ecosystem models or remote-sensing products. Nonetheless, direct application at larger scales requires caution: the flux footprint can expand under stable conditions or complex terrain, and one-year dataset may not capture interannual variability in crop rotations or extreme weather. Moreover, by focusing on atmospheric NEE, other carbon budget components (soil carbon changes, dissolved carbon losses, biomass exports) are omitted. Without coordinated soil sampling, stream water monitoring and harvest accounting, full budget closure is not achieved. The reliability of the RF gap-filling also depends on high-quality, representative training data; noisy measurement periods (e.g. storm-induced artifacts) degrade model performance, and models trained under one regime may not generalize without retraining.

Future efforts should address these limitations by integrating dynamic footprint modelling, extending monitoring across crop rotations and climate gradients, and including complementary soil and aquatic measurements. Such efforts would enable truly field-resolved carbon budgets that capture all relevant pathways and inform both scientific understanding and policy decisions.

5 Conclusions

This study illustrates that a cost-effective, single-tower EC system, when paired with sector-specific Random Forest modelling, can robustly capture the seasonal dynamics and annual carbon budgets of diverse agroecosystems. Sector-specific models revealed detailed phenological uptake peaks, management-driven flux reversals, and distinct responses to drought, while minimizing the propagation of anomalous data in final budget estimates. Although footprint uncertainties, dataset duration, and incomplete carbon-pool accounting present challenges, our approach offers a scalable template for integrating high-resolution flux observations into larger-scale carbon inventories. By broadening spatial coverage, extending temporal observation, and integrating soil and hydrological fluxes, future implementations can enhance the precision and comprehensiveness of agricultural carbon accounting, supporting both adaptive management and climate-mitigation policies.

Appendix A

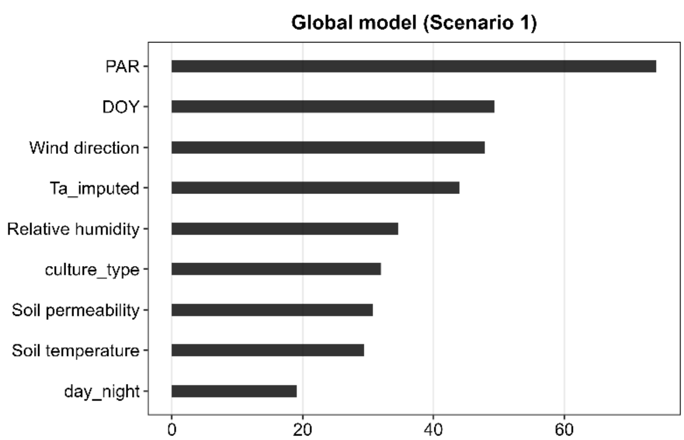

https://doi.org/10.5194/egusphere-2026-524
Preprint. Discussion started: 10 February 2026

Figure A1. Variable importance of the global model (Scenario 1), expressed as percentage increase in mean squared error (%IncMSE)

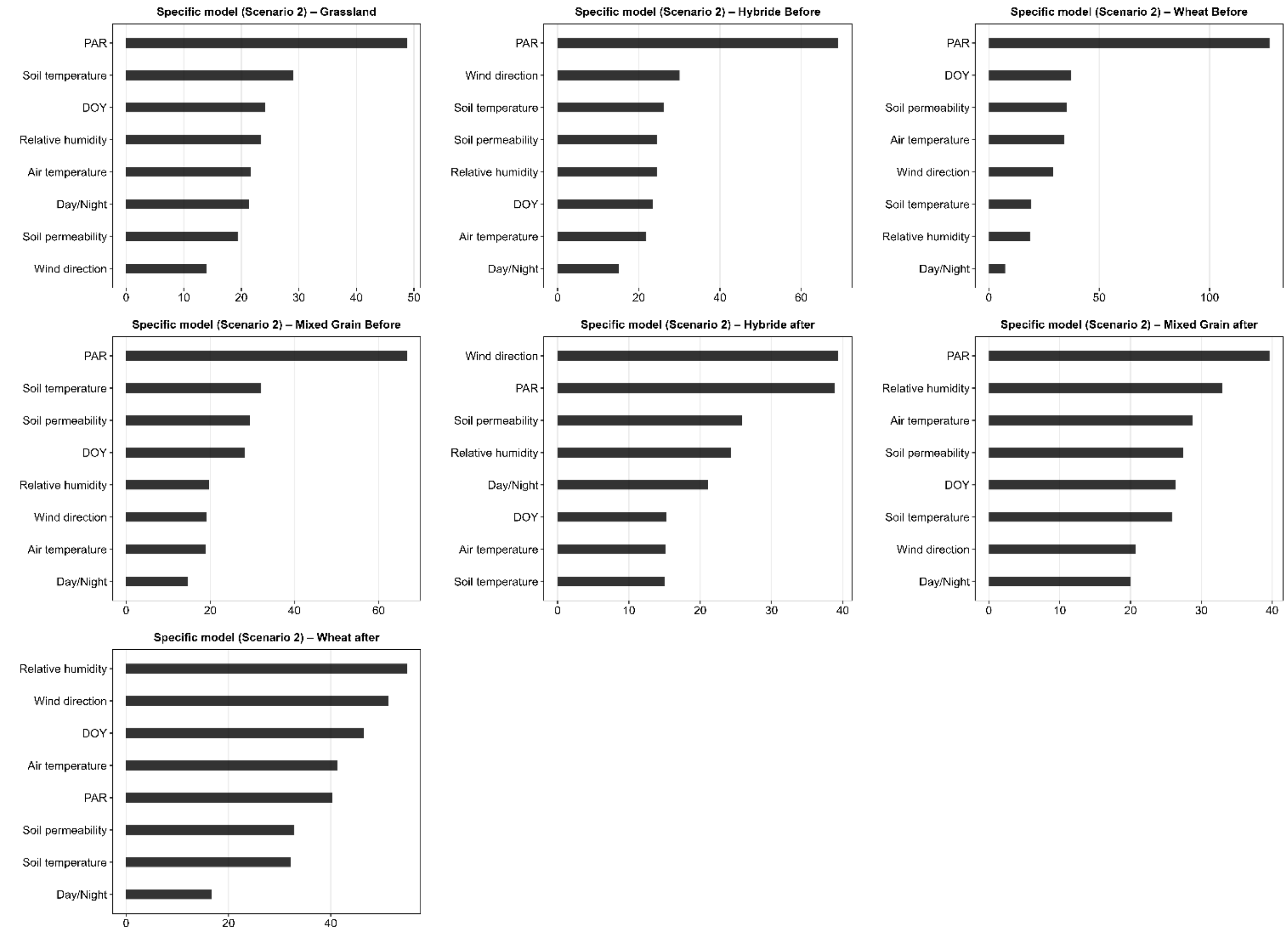

Figure A2. Variable importance across individual models in Scenario 2, expressed as percentage increase in mean squared error (%IncMSE)

Code/Data availability

All raw data can be provided by the corresponding authors upon request.

Author contribution

PP, EL, CP designed the study. PP, CD obtained the funding. PP, CP, JD performed the field work (EC tower deployment, maintenance, data retrieval). CP, PP, EL investigated and processed the data. PP, EL, NV, SB provided resources for data analysis. CP, PP, EL, NV, VM validated the data. CP made the graphics, wrote the draft. CP, PP led the review process assisted by CD, NV, OP.

Competing interests

The authors declare that they have no conflict of interest.

Acknowledgements

This work is a contribution of Camille Pery's two years work-study contract at Ifremer (Sept. 2022-Sept. 2024) in relationships with the LRTZC project (2019-2027: *La Rochelle Territoire Zero Carbone,* PIA TIGA #25875420; Caisse des Dépôts, Région Nouvelle-Aquitaine) and related to the ANR-22-PEXF-0006 - CarboNium project. We are grateful to our Ifremer colleague Louis Costes for his help in setting up the EC station, and to Wilfried Guignard and Rodolphe Pouponnot for the culture (management) information they provided us. We thank Maxime Paschal for his work on NDVI data during his internship and Nicolas Lachaussée for organizing drone flights.

References

Bajgain, R., Xiao, X., Basara, J., Wagle, P., Zhou, Y., Mahan, H., Gowda, P., McCarthy, H. R., Northup, B., Neel, J., and Steiner, J.: Carbon dioxide and water vapor fluxes in winter wheat and tallgrass prairie in central Oklahoma, Sci. Total Environ., 644, 1511–1524, https://doi.org/10.1016/j.scitotenv.2018.07.010, 2018.

Baldocchi, D. D.: How eddy covariance flux measurements have contributed to our understanding of Global Change Biology, Glob. Change Biol., 26, 242–260, https://doi.org/10.1111/gcb.14807, 2020.

Barr, A. G., Richardson, A. D., Hollinger, D. Y., Papale, D., Arain, M. A., Black, T. A., Bohrer, G., Dragoni, D., Fischer, M. L., Gu, L., Law, B. E., Margolis, H. A., McCaughey, J. H., Munger, J. W., Oechel, W., and Schaeffer, K.: Use of change-point detection for friction–velocity threshold evaluation in eddy-covariance studies, Agric. For. Meteorol., 171–172, 31–45, https://doi.org/10.1016/j.agrformet.2012.11.023, 2013.

Bou-Zeid, E., Anderson, W., Katul, G. G., and Mahrt, L.: The Persistent Challenge of Surface Heterogeneity in Boundary-Layer Meteorology: A Review, Bound.-Layer Meteorol., 177, 227–245, https://doi.org/10.1007/s10546-020-00551-8, 2020.

Breiman, L.: Random Forests, Mach. Learn., 45, 5–32, https://doi.org/10.1023/A:1010933404324, 2001.

Burba, G.: Eddy Covariance Method for Scientific, Industrial, Agricultural and Regulatory Applications: A Field Book on Measuring Ecosystem Gas Exchange and Areal Emission Rates, https://doi.org/10.13140/RG.2.1.4247.8561, 2013.

Butzer, K. W.: French Wetland Agriculture in Atlantic Canada and Its European Roots: Different Avenues to Historical Diffusion, Ann. Assoc. Am. Geogr., 92, 451–470, https://doi.org/10.1111/1467-8306.00299, 2002.

Coignot, E., Polsenaere, P., Soletchnik, P., Le Moine, O., Souchu, P., Joyeux, E., Le Roy, Y., Guéret, J.-P., Froud, L., Gallais, R., Chourré, E., Chaigneau, L., Soletchnik, P., Le Moine, O., Souchu, P., Joyeux, E., Le Roy, Y., Guéret, J.-P., Froud, L., Gallais, R., Chourré, E., and Chaigneau, L.: Variabilité spatio-temporelle des nutriments et du carbone et flux associés le long d'un continuum terrestre-aquatique tempéré (Marais poitevin – Baie de l'Aiguillon – Pertuis Breton), 2020.

Drewer, J., Anderson, M., Levy, P. E., Scholtes, B., Helfter, C., Parker, J., Rees, R. M., and Skiba, U. M.: The impact of ploughing intensively managed temperate grasslands on N2O, CH4 and CO2 fluxes, Plant Soil, 411, 193–208, https://doi.org/10.1007/s11104-016-3023-x, 2017.

Flanagan, L. B. and Adkinson, A. C.: Interacting controls on productivity in a northern Great Plains grassland and implications for response to ENSO events, Glob. Change Biol., 17, 3293–3311, https://doi.org/10.1111/j.1365-2486.2011.02461.x, 2011.

Friedlingstein, P., O'Sullivan, M., Jones, M. W., Andrew, R. M., Hauck, J., Landschützer, P., Le Quéré, C., Li, H., Luijkx, I. T., Olsen, A., Peters, G. P., Peters, W., Pongratz, J., Schwingshackl, C., Sitch, S., Canadell, J. G., Ciais, P., Jackson, R. B., Alin, S. R., Arneth, A., Arora, V., Bates, N. R., Becker, M., Bellouin, N., Berghoff, C. F., Bittig, H. C., Bopp, L., Cadule, P., Campbell, K., Chamberlain, M. A., Chandra, N., Chevallier, F., Chini, L. P., Colligan, T., Decayeux, J., Djeutchouang, L. M., Dou, X., Duran Rojas, C., Enyo, K., Evans, W., Fay, A. R., Feely, R. A., Ford, D. J., Foster, A., Gasser, T., Gehlen, M., Gkritzalis, T., Grassi, G., Gregor, L., Gruber, N., Gürses, Ö., Harris, I., Hefner, M., Heinke, J., Hurtt, G. C., Iida, Y., Ilyina, T., Jacobson, A. R., Jain, A. K., Jarníková, T., Jersild, A., Jiang, F., Jin, Z., Kato, E., Keeling, R. F., Klein Goldewijk, K., Knauer, J., Korsbakken, J. I., Lan, X., Lauvset, S. K., Lefèvre, N., Liu, Z., Liu, J., Ma, L., Maksyutov, S., Marland, G., Mayot, N., McGuire, P. C., Metzl, N., Monacci, N. M., Morgan, E. J., Nakaoka, S.-I., Neill, C., Niwa, Y., Nützel, T., Olivier, L., Ono, T., Palmer, P. I., Pierrot, D., Qin, Z., Resplandy, L., Roobaert, A., Rosan, T. M., Rödenbeck, C., Schwinger, J., Smallman, T. L., Smith, S. M., Sospedra-Alfonso, R., Steinhoff, T., et al.: Global Carbon Budget 2024, Earth Syst. Sci. Data, 17, 965–1039, https://doi.org/10.5194/essd-17-965-2025, 2025.

Gao, D., Yao, J., Yu, S., Ma, Y., Li, L., and Gao, Z.: Eddy Covariance CO2 Flux Gap Filling for Long Data Gaps: A Novel Framework Based on Machine Learning and Time Series Decomposition, Remote Sens., 15, 2695, https://doi.org/10.3390/rs15102695, 2023.

Gash, J. H. C. and Culf, A. D.: Applying a linear detrend to eddy correlation data in realtime, Bound.-Layer Meteorol., 79, 301–306, https://doi.org/10.1007/BF00119443, 1996.

Gilmanov, T. G., Verma, S. B., Sims, P. L., Meyers, T. P., Bradford, J. A., Burba, G. G., and Suyker, A. E.: Gross primary production and light response parameters of four Southern Plains ecosystems estimated using long-term CO2-flux tower measurements, Glob. Biogeochem. Cycles, 17, undefined-undefined, https://doi.org/10.1029/2002gb002023, 2003.

Gu, L., Falge, E. M., Boden, T., Baldocchi, D. D., Black, T. A., Saleska, S. R., Suni, T., Verma, S. B., Vesala, T., Wofsy, S. C., and Xu, L.: Objective threshold determination for nighttime eddy flux filtering, Agric. For. Meteorol., 128, 179–197, https://doi.org/10.1016/j.agrformet.2004.11.006, 2005.

Heimsch, L., Lohila, A., Tuovinen, J.-P., Vekuri, H., Heinonsalo, J., Nevalainen, O., Korkiakoski, M., Liski, J., Laurila, T., and Kulmala, L.: Carbon dioxide fluxes and carbon balance of an agricultural grassland in southern Finland, Biogeosciences, 18, 3467–3483, https://doi.org/10.5194/bg-18-3467-2021, 2021.

Hernandez Rodriguez, L. C., Goodwell, A. E., and Kumar, P.: Inside the flux footprint: The role of organized land cover heterogeneity on the dynamics of observed land-atmosphere exchange fluxes, Front. Water, 5, https://doi.org/10.3389/frwa.2023.1033973, 2023.

Jaksic, V., Kiely, G., Albertson, J., Oren, R., Katul, G., Leahy, P., and Byrne, K. A.: Net ecosystem exchange of grassland in contrasting wet and dry years, Agric. For. Meteorol., 139, 323–334, https://doi.org/10.1016/j.agrformet.2006.07.009, 2006.

Knauer, J., Zaehle, S., Medlyn, B. E., Reichstein, M., Williams, C. A., Migliavacca, M., De Kauwe, M. G., Werner, C., Keitel, C., Kolari, P., Limousin, J.-M., and Linderson, M.-L.: Towards physiologically meaningful water-use efficiency estimates from eddy covariance data, Glob. Change Biol., 24, 694–710, https://doi.org/10.1111/gcb.13893, 2018.

Kowalski, S., Sartore, M., Burlett, R., Berbigier, P., and Loustau, D.: The annual carbon budget of a French pine forest (Pinus pinaster) following harvest, Glob. Change Biol., 9, 1051–1065, https://doi.org/10.1046/j.1365-2486.2003.00627.x, 2003.

Kumari, S., Kambhammettu, B. V. N. P., and Niyogi, D.: Sensitivity of Analytical Flux Footprint Models in Diverse Source-Receptor Configurations: A Field Experimental Study, J. Geophys. Res. Biogeosciences, 125, e2020JG005694, https://doi.org/10.1029/2020JG005694, 2020.

Liebman, M. and Dyck, E.: Crop Rotation and Intercropping Strategies for Weed Management, Ecol. Appl., 3, 92–122, https://doi.org/10.2307/1941795, 1993.

Liu, L., Zhou, W., Guan, K., Peng, B., Xu, S., Tang, J., Zhu, Q., Till, J., Jia, X., Jiang, C., Wang, S., Qin, Z., Kong, H., Grant, R., Mezbahuddin, S., Kumar, V., and Jin, Z.: Knowledge-guided machine learning can improve carbon cycle quantification in agroecosystems, Nat. Commun., 15, 357, https://doi.org/10.1038/s41467-023-43860-5, 2024.

Lloyd, J. and Taylor, J. A.: On the Temperature Dependence of Soil Respiration, Funct. Ecol., 8, 315–323, https://doi.org/10.2307/2389824, 1994.

Mahecha, M. D., Reichstein, M., Carvalhais, N., Lasslop, G., Lange, H., Seneviratne, S. I., Vargas, R., Ammann, C., Arain, M. A., Cescatti, A., Janssens, I. A., Migliavacca, M., Montagnani, L., and Richardson, A. D.: Global Convergence in the Temperature Sensitivity of Respiration at Ecosystem Level, Science, 329, 838–840, https://doi.org/10.1126/science.1189587, 2010.

Mayen, J., Polsenaere, P., Lamaud, É., Arnaud, M., Kostyrka, P., Bonnefond, J.-M., Geairon, P., Gernigon, J., Chassagne, R., Lacoue-Labarthe, T., Regaudie de Gioux, A., and Souchu, P.: Atmospheric CO_2 exchanges measured by eddy covariance over a temperate salt marsh and influence of environmental controlling factors, Biogeosciences, 21, 993–1016, https://doi.org/10.5194/bg-21-993-2024, 2024.

Mayen, J., Polsenaere, P., Regaudie de Gioux, A., Deborde, J., Collin, K., Le Merrer, Y., Foucault, É., Ouisse, V., André, L., Arnaud, M., Kostyrka, P., Lamaud, É., Abril, G., and Souchu, P.: Aquatic metabolism influences temporal variations of water carbon and atmospheric carbon dioxide fluxes in a temperate salt marsh, Biogeosciences, 22, 5387–5411, https://doi.org/10.5194/bg-22-5387-2025, 2025.

Moreaux, V., Longdoz, B., Berveiller, D., Delpierre, N., Dufrêne, E., Bonnefond, J.-M., Chipeaux, C., Joffre, R., Limousin, J.-M., Ourcival, J.-M., Klumpp, K., Darsonville, O., Brut, A., Tallec, T., Ceschia, E., Panthou, G., and Loustau, D.: Environmental control of land-atmosphere CO2 fluxes from temperate ecosystems: a statistical approach based on homogenized time series from five land-use types, Tellus B Chem. Phys. Meteorol., 72, 2020.

Novick, K. A., Ficklin, D. L., Stoy, P. C., Williams, C. A., Bohrer, G., Oishi, A. C., Papuga, S. A., Blanken, P. D., Noormets, A., Sulman, B. N., Scott, R. L., Wang, L., and Phillips, R. P.: The increasing importance of atmospheric demand for ecosystem water and carbon fluxes, Nat. Clim. Change, 6, 1023–1027, https://doi.org/10.1038/nclimate3114, 2016.

Papale, D., Reichstein, M., Aubinet, M., Canfora, E., Bernhofer, C., Kutsch, W., Longdoz, B., Rambal, S., Valentini, R., Vesala, T., and Yakir, D.: Towards a standardized processing of Net Ecosystem Exchange measured with eddy covariance technique: algorithms and uncertainty estimation, Biogeosciences, 3, 571–583, https://doi.org/10.5194/bg-3-571-2006, 2006.

Reichstein, M., Falge, E., Baldocchi, D., Papale, D., Aubinet, M., Berbigier, P., Bernhofer, C., Buchmann, N., Gilmanov, T., Granier, A., Grünwald, T., Havránková, K., Ilvesniemi, H., Janous, D., Knohl, A., Laurila, T., Lohila, A., Loustau, D., Matteucci, G., Meyers, T., Miglietta, F., Ourcival, J.-M., Pumpanen, J., Rambal, S., Rotenberg, E., Sanz, M., Tenhunen, J., Seufert, G., Vaccari, F., Vesala, T., Yakir, D., and Valentini, R.: On the separation of net ecosystem exchange into assimilation

https://doi.org/10.5194/egusphere-2026-524
Preprint. Discussion started: 10 February 2026

and ecosystem respiration: review and improved algorithm, Glob. Change Biol., 11, 1424–1439, https://doi.org/10.1111/j.1365-2486.2005.001002.x, 2005.

Reichstein, M., Ciais, P., Papale, D., Valentini, R., Running, S., Viovy, N., Cramer, W., Granier, A., Ogée, J., Allard, V., Aubinet, M., Bernhofer, Chr., Buchmann, N., Carrara, A., Grünwald, T., Heimann, M., Heinesch, B., Knohl, A., Kutsch, W., Loustau, D., Manca, G., Matteucci, G., Miglietta, F., Ourcival, J. m., Pilegaard, K., Pumpanen, J., Rambal, S., Schaphoff, S., Seufert, G., Soussana, J.-F., Sanz, M.-J., Vesala, T., and Zhao, M.: Reduction of ecosystem productivity and respiration during the European summer 2003 climate anomaly: a joint flux tower, remote sensing and modelling analysis, Glob. Change Biol., 13, 634–651, https://doi.org/10.1111/j.1365-2486.2006.01224.x, 2007.

Reynolds: I. On the theory of lubrication and its application to Mr. Beauchamp tower's experiments, including an experimental determination of the viscosity of olive oil, Proc. R. Soc. Lond., 40, 191–203, https://doi.org/10.1098/rspl.1886.0021, 1886.

Schmidt, M., Reichenau, T. G., Fiener, P., and Schneider, K.: The carbon budget of a winter wheat field: An eddy covariance analysis of seasonal and inter-annual variability, Agric. For. Meteorol., 165, 114–126, https://doi.org/10.1016/j.agrformet.2012.05.012, 2012.

Schmidt, M. W. I., Torn, M. S., Abiven, S., Dittmar, T., Guggenberger, G., Janssens, I. A., Kleber, M., Kögel-Knabner, I., Lehmann, J., Manning, D. A. C., Nannipieri, P., Rasse, D. P., Weiner, S., and Trumbore, S. E.: Persistence of soil organic matter as an ecosystem property, Nature, 478, 49–56, https://doi.org/10.1038/nature10386, 2011.

Senapati, N., Chabbi, A., Gastal, F., Smith, P., Mascher, N., Loubet, B., Cellier, P., and Naisse, C.: Net carbon storage measured in a mowed and grazed temperate sown grassland shows potential for carbon sequestration under grazed system, Carbon Manag., 5, 131, https://doi.org/10.1080/17583004.2014.912863, 2014.

Tilman, D., Reich, P. B., and Knops, J. M. H.: Biodiversity and ecosystem stability in a decade-long grassland experiment, Nature, 441, 629–632, https://doi.org/10.1038/nature04742, 2006.

Vickers, D. and Mahrt, L.: Quality Control and Flux Sampling Problems for Tower and Aircraft Data, 1997.

Wagle, P., Gowda, P. H., Northup, B. K., Turner, K. E., Neel, J. P. S., Manjunatha, P., and Zhou, Y.: Variability in carbon dioxide fluxes among six winter wheat paddocks managed under different tillage and grazing practices, Atmos. Environ., 185, 100–108, https://doi.org/10.1016/j.atmosenv.2018.05.003, 2018.

Wang, K., Liu, C., Zheng, X., Pihlatie, M., Li, B., Haapanala, S., Vesala, T., Liu, H., Wang, Y., Liu, G., and Hu, F.: Comparison between eddy covariance and automatic chamber techniques for measuring net ecosystem exchange of carbon dioxide in cotton and wheat fields, Biogeosciences, 10, 6865–6877, https://doi.org/10.5194/bg-10-6865-2013, 2013.

Wohlfahrt, G. and Gu, L.: The many meanings of gross photosynthesis and their implication for photosynthesis research from leaf to globe, Plant Cell Environ., 38, 2500–2507, https://doi.org/10.1111/pce.12569, 2015.

Wu, L., Miao, H., and Liu, T.: Development in Agricultural Ecosystems' Carbon Emissions Research: A Visual Analysis Using CiteSpace, Agronomy, 14, 1288, https://doi.org/10.3390/agronomy14061288, 2024.

Zeng, J., Matsunaga, T., Tan, Z.-H., Saigusa, N., Shirai, T., Tang, Y., Peng, S., and Fukuda, Y.: Global terrestrial carbon fluxes of 1999–2019 estimated by upscaling eddy covariance data with a random forest, Sci. Data, 7, 313, https://doi.org/10.1038/s41597-020-00653-5, 2020.

Zomer, R. J., Bossio, D. A., Sommer, R., and Verchot, L. V.: Global Sequestration Potential of Increased Organic Carbon in Cropland Soils, Sci. Rep., 7, 15554, https://doi.org/10.1038/s41598-017-15794-8, 2017.